A Mach-Sensitive Implicit-Explicit Scheme Adapted to Compressible Multi-scale Flows

David Iampietro, Frédéric Daude, Pascal Galon, Jean-Marc Hérard

A Mach-Sensitive Implicit-Explicit Scheme Adapted to Compressible Multi-scale Flows

D. Iampietro [*1,3,4], F. Daude [†1,3], P. Galon [‡3,5], and J-M Hérard [§2,4]

[1] *EDF lab Saclay, 7 boulevard Gaspard Monge 92120 Palaiseau, France*
[2] *EDF lab Chatou, 6 Quai Watier 78400 Chatou, France*
[3] *IMSIA, UMR EDF/CNRS/CEA/ENSTA 9219 Université Paris Saclay 828 Boulevard des Maréchaux 91762 Palaiseau Cedex, France*
[4] *I2M, UMR CNRS 7373 Technopôle Château-Gombert 39, rue F. Joliot Curie 13453 Marseille Cedex 13, France*
[5] *CEA DEN/DANS/DM2S/SEMT/DYN, D36 91190 Saclay, France*

May 31, 2017

Abstract

The method presented below focuses on the numerical approximation of the Euler compressible system. It pursues a two-fold objective: being able to accurately follow slow material waves as well as strong shock waves in the context of low Mach number flows. The resulting implicit-explicit fractional step approach leans on a dynamic splitting designed to react to the time fluctuations of the maximal flow Mach number. Would the latter rise suddenly, the IMEX scheme, so far driven by a material-wave Courant number, would turn into a time-explicit approximate Riemann solver constrained by an acoustic-wave Courant number. One dimensional low Mach number test cases involving single or multiple waves confirm that the present approach is as accurate and efficient as an IMEX Lagrange-Projection method. Besides, a pragmatic stability study suggests that the resulting IMEX scheme is stable, whatever the Mach number, for a material-wave Courant number of order unity.

1 Introduction

The present work deals with the construction of a time implicit-explicit scheme providing a sketch of answer to cope with multi-scale wave scenarios and more specifically with what is called a *condensation induced water hammer* (CIWH).

[*] david.iampietro@edf.fr; Corresponding author
[†] frederic.daude@edf.fr
[‡] pascal.galon@cea.fr
[§] jean-marc.herard@edf.fr

Indeed, in the very first instants of this phenomenon, one is interested in following a slow interface between hot vapor and cooler liquid water. Since the speed of such a material wave is of the order of $1\ m.s^{-1}$, which is considerably smaller than the acoustic wave speeds in both phases, the interface dynamics is typical from a low Mach number flow. Nonetheless, as time goes on, shear instabilities and steep temperature gradients entail the trapping and then the sudden condensation of vapor pockets leading to the production of strong shock waves in the liquid phase.

The objective is thus to design a numerical scheme accurate for material waves in a low Mach number flow while being able to capture high pressure gradients.

On one hand, fulfilling both aims might seem contradictory if one considers the Euler or Navier-Stokes incompressible systems since their divergence-free constraint prohibits any compressible effects and hence the occurrence of compressive shock waves. On the other hand, the pioneering works of Joukowski [25] and Allievi [1] state that, at constant temperature, pressure jumps in a low Mach number compressible flow are given by: $\Delta p = \rho^0\, c^0\, \Delta u$; with ρ^0 (respectively c^0) the constant density (respectively the constant speed of sound) of the fluid. See also [17] for a review of the water hammer theory. Thus, in the case of liquid water, at $295\,K$, $\rho^0 \approx 10^3\ kg.m^{-3}$, $c^0 \approx 1.5 \times 10^3\ m.s^{-1}$. If one assumes that $\Delta u \approx 1\ m.s^{-1}$, pressure jumps amplitude is of 15 bar which is the order of magnitude observed experimentally in [32].

From a numerical point of view, different strategies have been adopted in order to be accurate on slow material waves in the case of low Mach number flows. Preconditioning methods stemming from [34] and improved in [20, 19, 29] aim at modifying the Jacobian eigenvalues of hyperbolic systems in order to get rid of their constraining acoustic part. Asymptotic preserving schemes (AP schemes), introduced by Jin in [24], are based on the identification of a non-stiff and a stiff part of hyperbolic systems. The latter is then discretized using a time-implicit method which allows the scheme to be consistent, at discrete level, with a targeted asymptotic continuous system as a scale parameter tends towards zero. Recently in [13, 21, 30, 15], different kinds of AP schemes have been derived to seize the incompressible limit of the Euler or the Navier-Stokes system as the flow Mach number tends towards zero. It results in an implicit-explicit (IMEX) algorithms providing a time-implicit discretization for the hydrodynamic pressure gradient, and a time-explicit discretization for the convective terms. Besides, if one considers the Courant number $\mathscr{C}$ based on the slowest material waves of the flow, a key property for the above AP schemes is also to remain stable for $\mathscr{C} \approx 1$ at any Mach numbers. This topical issue has been explored using the "modified equation" tools as well as the spectral theory by Noelle an his collaborators in [31, 37]. See also [36] in which the AP property as well as the Mach-uniform stability property has been proved for a Lagrange-Projection method described in [8].

If the above tracks of reflection constitute substantial breakthroughs for the material waves representation in the context of low Mach numbers flows, no satisfying solution has been yet found in order to dynamically capture shock waves if they suddenly appear in such a configuration.

Continuing ideas suggested in [11, 23], the present work derives an IMEX scheme based on a Mach-sensitive splitting of the Euler system. Such a splitting stems from the pioneering work of Baraille and co-authors [4]. The resulting fractional step approach evolves dynamically in time thanks to a parameter measuring the instantaneous maximal Mach number of the flow. Particularly, starting from a completely decoupled IMEX formulation with $\mathscr{C} \approx 1$, it offers the possibility to retrieve a time-explicit scheme for the overall Euler system if a sudden rise of the Mach number is detected. The CFL condition adapts itself and is re-based on the fastest physically relevant wave speed, i.e. the

acoustic one. Thus, shock waves can be optimally captured.

The first section of this article is a condensed presentation of the Mach-sensitive splitting fully described in [23]. The readers are notably referred to this work for the construction of a time-explicit scheme for both convective and acoustic parts of the Mach-sensitive splitting. Hence, the second section of the present study is entirely dedicated to the derivation of a time-implicit scheme related to the acoustic part of the splitting. It leans on the relaxation schemes theory and particularly on a Suliciu-like relaxation procedure detailed in [33, 6, 11, 10]. Eventually the last two sections aggregate three types of one dimensional numerical results. A first part describes briefly the effect of the Courant number when an IMEX scheme is triggered on an isolated shock or contact waves in the context of a low Mach number flow. In a second time, the accuracy and the efficiency of the present approach are compared with the Lagrange-Projection fractional step method described in [8]. Finally, the Mach-uniformity of the stability condition for $\mathscr{C} \approx 1$ is tested and analyzed.

2 A Mach-Sensitive Fractional Step Approach

The present work focuses on the Euler compressible system. However its extension to the two-phase Homogeneous Equilibrium Model (HEM, [9]) in which both phases have the same velocity $\mathbf{u}$, pressure p, temperature T and chemical potential is straightforward since it results in the same conservation law structure, namely:

$$\partial_t \rho + \underline{\nabla} \cdot (\rho \mathbf{u}) = 0, \tag{1a}$$
$$\partial_t (\rho \mathbf{u}) + \underline{\nabla} \cdot (\rho \mathbf{u} \otimes \mathbf{u} + p \mathbf{I}) = \mathbf{0}, \tag{1b}$$
$$\partial_t (\rho e) + \underline{\nabla} \cdot ((\rho e + p) \mathbf{u}) = 0, \tag{1c}$$
$$e = \frac{|\mathbf{u}|^2}{2} + \varepsilon, \ \varepsilon = \varepsilon^{EOS}(\rho, p), \tag{1d}$$
$$(\rho c)^2 = \left(\partial_p \varepsilon_{|\rho}\right)^{-1} \left(p - \rho^2 \partial_\rho \varepsilon_{|p}\right), \tag{1e}$$

with ρ the density of the mixture and ε its specific internal energy. The function $\varepsilon^{EOS}(.,.)$ defines the equation of state between the thermodynamic variables while c is the sound speed involved in the nonlinear wave propagation.

As described in [23], it is possible to derive a scheme able to deal with highly compressible flows as well as low Mach number flows by splitting the system (1) into a convective ($\mathcal{C}$) and an acoustic ($\mathcal{A}$) subsystem:

$$\mathcal{C} : \begin{cases} \partial_t \rho + \underline{\nabla} \cdot (\rho \mathbf{u}) = 0, \\ \partial_t (\rho \mathbf{u}) + \underline{\nabla} \cdot \left(\rho \mathbf{u} \otimes \mathbf{u} + \mathscr{E}_0^2(t)\, p \mathbf{I}\right) = \mathbf{0}, \\ \partial_t (\rho e) + \underline{\nabla} \cdot \left((\rho e) + \mathscr{E}_0^2(t)\, p) \mathbf{u}\right) = 0, \end{cases} \tag{2}$$

$$\mathcal{A} : \begin{cases} \partial_t \rho = 0, \\ \partial_t (\rho \mathbf{u}) + \underline{\nabla} \cdot \left((1 - \mathscr{E}_0^2(t))\, p \mathbf{I}\right) = \mathbf{0}, \\ \partial_t (\rho e) + \underline{\nabla} \cdot \left((1 - \mathscr{E}_0^2(t))\, p \mathbf{u}\right) = 0. \end{cases} \tag{3}$$

Here, $\mathscr{E}_0(t) \in]0, 1]$ is a dynamic splitting parameter designed to be equal to one in the case of sonic or

supersonic flows or equal to the maximal flow Mach number in the case of subsonic flows:

$$\begin{aligned} \mathscr{E}_0(t) &= \max\left(M_{inf},\, \min\left(M_{max}(t),\, 1\right)\right), \\ M_{max}(t) &= \sup_{x\in\Omega}\left(M(x,t) = \frac{|u(x,t)|}{c(x,t)}\right), \end{aligned} \tag{4}$$

with M_{inf} a given lower bound preventing $\mathscr{E}_0(t)$ from being exactly equal to zero. As shown in [23], both subsystems are hyperbolic for a stiffened gas thermodynamics provided that the pressure remains positive throughout space and time. In one dimension, their eigenvalues are:

$$\begin{aligned} \lambda_1^{\mathcal{C}} &= u - \mathscr{E}_0\, c_{\mathcal{C}} && \leq \lambda_2^{\mathcal{C}} = u \leq \lambda_3^{\mathcal{C}} = u + \mathscr{E}_0\, c_{\mathcal{C}}, \\ \lambda_1^{\mathcal{A}} &= -\left(1-\mathscr{E}_0^2\right)\, c_{\mathcal{A}} && \leq \lambda_2^{\mathcal{A}} = 0 \leq \lambda_3^{\mathcal{A}} = \left(1-\mathscr{E}_0^2\right)\, c_{\mathcal{A}}, \end{aligned} \tag{5}$$

with $c_{\mathcal{C}}$ (respectively $c_{\mathcal{A}}$) the convective (respectively the acoustic) celerity defined by:

$$\begin{aligned} \left(\rho\, c_{\mathcal{C}}\left(\rho,\, p\right)\right)^2 &= \left(\partial_p\, \varepsilon_{|\rho}\right)^{-1}\, \left(\mathscr{E}_0^2\, p - \,\rho^2\, \partial_\rho\, \varepsilon_{|p}\right), \\ \left(\rho\, c_{\mathcal{A}}\left(\rho,\, p\right)\right)^2 &= \left(\partial_p\, \varepsilon_{|\rho}\right)^{-1}\, p, \end{aligned} \tag{6}$$

and:

$$\left(c_{\mathcal{C}}\right)^2 + \left(1-\mathscr{E}_0^2\right)\, \left(c_{\mathcal{A}}\right)^2 = c^2. \tag{7}$$

What is more, the 1-wave and 3-wave of both subsystems are associated to genuinely non-linear fields whereas the 2-wave field is linearly degenerate.

It can be noticed that, when the Mach number is small so that $\mathscr{E}_0(t)$ is close to zero, pressure terms completely disappear from the subsystem $\mathcal{C}$ which only conserves the convective spatial operator $\underline{\nabla}\cdot(\mathbf{u}\ *)$. Pressure terms are retrieved in the subsystem $\mathcal{A}$ which turns out to hold most of the acoustic effects. That is why, in the case of low Mach number flows, if the physics of interest is essentially related to material waves propagating at speed $|u| \ll c$, a time-implicit discretization will be provided for subsystem $\mathcal{A}$ while $\mathcal{C}$ will be solved with a time-explicit scheme.

Indeed, define Δx the space step of the computational domain. If Δt is the time step guaranteeing the stability of the numerical scheme, one can formally introduce several Courant numbers related to the above wave speeds, namely:

$$\begin{aligned} \mathscr{C}_E &= \frac{\left(|u| + c\right)\Delta t}{\Delta x} && \text{Euler Courant number,} \\ \mathscr{C}_{|u|} &= \frac{|u|\ \Delta t}{\Delta x} && \text{Convective Courant number,} \\ \mathscr{C}_{\mathcal{C}} &= \frac{\left(|u| + \mathscr{E}_0\, c_{\mathcal{C}}\right)\Delta t}{\Delta x} && \text{Courant number related to } \mathcal{C}, \\ \mathscr{C}_{\mathcal{A}} &= \frac{\left(\left(1-\mathscr{E}_0^2\right) c_{\mathcal{A}}\right)\Delta t}{\Delta x} && \text{Courant number related to } \mathcal{A}. \end{aligned} \tag{8}$$

By using a time-implicit scheme for the resolution of the subsystem $\mathcal{A}$, one seeks to be relieved from most of the time-explicit stability condition: $\mathscr{C}_E < 1$. Particularly, if the scheme allows to fulfill

$\mathscr{C}_{|u|} \approx 1$, one expects a substantial drop of the numerical diffusion holding on the material waves propagating at speed $|u|$.

We refer the readers to [23] for the complete study of both continuous subsystems $\mathcal{C}$ and $\mathcal{A}$ as well as the derivation of *a full time-explicit* fractional step involving relaxation schemes. A short description of the time-explicit convective flux related to the subsystem $\mathcal{C}$ is written in Appendix A.

In the following, the derivation of the $\mathcal{A}$-time-implicit $\mathcal{C}$-time-explicit fractional step approach is presented. As the $\mathcal{C}$-time-explicit scheme described in [23] is given in Appendix A, focus is only given on the $\mathcal{A}$-time-implicit integration.

3 A Sulicu-like Relaxation Scheme for the Acoustic Subsystem

Let us introduce a new Suliciu-like *relaxation* subsystem $\mathcal{A}^\mu$ as:

$$\mathcal{A}^\mu : \begin{cases} \partial_t \rho = 0, \\ \partial_t (\rho u) + \partial_x \left((1 - \mathscr{E}_0^2(t)) \Pi \right) = 0, \\ \partial_t (\rho \Pi) + \partial_x \left((1 - \mathscr{E}_0^2(t)) a_{\mathcal{A}}^2 u \right) = \dfrac{\rho (p - \Pi)}{\mu}, \\ \partial_t (\rho e) + \partial_x \left((1 - \mathscr{E}_0^2(t)) \Pi u \right) = 0, \end{cases} \quad (\mathcal{A}^\mu)^{NC} : \begin{cases} \partial_t \tau = 0, \\ \partial_t u + (1 - \mathscr{E}_0^2(t)) \tau \partial_x \Pi = 0, \\ \partial_t \Pi + (1 - \mathscr{E}_0^2(t)) a_{\mathcal{A}}^2 \tau \partial_x u = \dfrac{(p - \Pi)}{\mu}, \\ \partial_t e + (1 - \mathscr{E}_0^2(t)) \tau \partial_x (\Pi u) = 0. \end{cases} \tag{9-10}$$

More details on relaxation schemes can be found in [33, 5, 10]. Moreover, the derivation of the above relaxation subsystem can be found in [23]. Recall that Π is the relaxation pressure forced to converge towards the real pressure p thanks to a source term of timescale $\mu \ll 1$. Besides, $a_{\mathcal{A}}$ is a relaxation constant encapsulating the thermodynamic nonlinearity. In order to provide sufficient diffusion to the relaxation subsystem, one can exhibit (see [35, 8, 23]) the following subcharacteristic condition:

$$a_{\mathcal{A}} > \rho c_{\mathcal{A}}. \tag{11}$$

Let us define $\tau = 1/\rho$ the specific volume. Using the fact that the density is independent of time, the relaxation subsystem $\mathcal{A}^\mu$ is equivalent to its non-conservative version $(\mathcal{A}^\mu)^{NC}$. Then, one can easily prove that the relaxation subsystem is hyperbolic, and that its eigenvalues are:

$$\lambda_1^{\mathcal{A},\mu} = -(1 - \mathscr{E}_0^2)\, a_{\mathcal{A}} \tau < \lambda_2^{\mathcal{A},\mu} = \lambda_3^{\mathcal{A},\mu} = 0 < \lambda_4^{\mathcal{A},\mu} = (1 - \mathscr{E}_0^2)\, a_{\mathcal{A}} \tau. \tag{12}$$

Besides all its characteristic fields are linearly degenerate. Let us now introduce W and R as:

$$\begin{aligned} W &= u - \Pi / a_{\mathcal{A}}, \\ R &= u + \Pi / a_{\mathcal{A}}. \end{aligned} \tag{13}$$

It is worth noticing that the non-conservative subsystem $(\mathcal{A}^\mu)^{NC}$ is equivalent to:

$$\begin{cases} \partial_t \tau = 0, \\ \partial_t W + \lambda_1^{\mathcal{A},\mu} \partial_x W = -\dfrac{(p - \Pi)}{a_{\mathcal{A}} \mu}, \\ \partial_t R + \lambda_4^{\mathcal{A},\mu} \partial_x R = \dfrac{(p - \Pi)}{a_{\mathcal{A}} \mu}, \\ \partial_t e + (1 - \mathscr{E}_0^2(t)) \tau \partial_x (\Pi u) = 0. \end{cases} \tag{14}$$

with $u(W,\,R) = (R+W)/2$ and $\Pi(W,\,R) = a_{\mathcal{A}}\,(R-W)/2$. Thus, W (respectively R) is constant along the 1-characteristic curves (respectively the 4-characteristic curves). What is more, it is a 1-strong Riemann invariant (respectively a 4-strong Riemann invariant) meaning that it is constant through the 2,3 and 4 waves (respectively the 1 and 2,3 waves). On Figure 1 the domains of invariance of R and W are drawn.

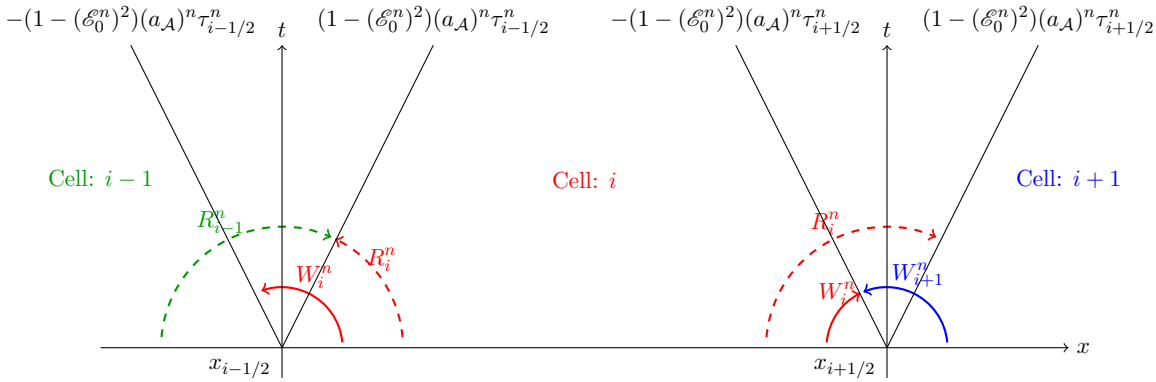

Figure 1: Strong Riemann Invariants Behaviors

As already noticed in [11, 18], if one formally removes the relaxation terms $\pm(p-\Pi)/(a_{\mathcal{A}}\,\mu)$ from the PDEs (14), the dynamics of W and R become totally uncoupled. Besides the energy flux depends only on these two quantities.

The time-implicit scheme for the subsystem $\mathcal{A}$ derived below is based on the extension of this property at the discrete level.

4 The Acoustic Time-Implicit Scheme

The numerical resolution of the acoustic relaxation subsystem $\mathcal{A}^\mu$ is split into two steps: the first one, sometimes called *the evolution step* corresponds to the resolution of the homogeneous subsystem where the term $(p-\Pi)/\mu$ has been removed. It becomes active afterwards during a *projection step* which, in our case, consists in solving: $\partial_t\,\Pi = (p-\Pi)\,/\mu$.

4.1 A One-dimensional Implicit-Solver for the Evolution Step

Suppose that the computational domain $\Omega = [0,\,L]$ is made of N_{cells} cells. Let us define $\Delta x = L/N_{cells}$ (respectively Δt) the space step (respectively the time step) of the scheme. For $i \in [1,..,\,N_{cells}]$ let us set $x_i = (i-1/2)\,\Delta x$, the coordinate of the cell center i and $x_{i+1/2} = x_i + \Delta x/2$, the coordinate of face $i+1/2$. Finally define $\Omega_i =]x_{i-1/2},\,x_{i+1/2}[$. Suppose that at time $t^n = n\,\Delta t$, the initial datum of $\mathcal{A}^\mu$ is piecewise continuous on $\sqcup_{i=1}^{N_{cells}}\,\Omega_i$. Then, by averaging the W-equation and the R-equation in

(14) over $\Omega_i \times]t^n,\, t^{n+} > t^n[$ one obtains:

$$\begin{aligned}
&\frac{W_i^{n+} - W_i^n}{\Delta t} - \frac{\left(1 - (\mathscr{E}_0^n)^2\right)\,(a_{\mathcal{A}})^n\,\tau_i^n}{\Delta x}\,\Big(W_{i+1/2}(t^n,\, t^{n+}) - W_{i-1/2}(t^n,\, t^{n+})\Big) = 0,\\
&\frac{R_i^{n+} - R_i^n}{\Delta t} + \frac{\left(1 - (\mathscr{E}_0^n)^2\right)\,(a_{\mathcal{A}})^n\,\tau_i^n}{\Delta x}\,\Big(R_{i+1/2}(t^n,\, t^{n+}) - R_{i-1/2}(t^n,\, t^{n+})\Big) = 0,
\end{aligned} \tag{15}$$

with W_i^n the spatial average over Ω_i at time t^n, $W_{i+1/2}(t^n,\, t^{n+}) = \Big(1/(t^{n+} - t^n)\Big) \times \displaystyle\int_{t^n}^{t^{n+}} \mathrm{W}(x_{i+1/2}/t)\, dt$, and $(a_{\mathcal{A}})^n = K \underset{i\in[1,\,N_{cells}]}{max} \left(\rho_i^n\,(c_{\mathcal{A}})_i^n\right),\ K > 1$, the discrete acoustic relaxation constant fulfilling inequality (11) throughout the whole computational domain. Eventually the Mach-sensitive discrete parameter is given by:

$$\begin{aligned}
\mathscr{E}_0^n &= \max\left(M_{inf},\, \min\left(M_{max}^n,\, 1\right)\right),\\
\text{with: } M_{max}^n &= \underset{i\in[1,\,N_{cells}]}{max} \left(\frac{u_i^n}{c_i^n}\right).
\end{aligned} \tag{16}$$

Remark 1. *Averaging over a non-conservative term:*

One can notice that, even if the R and W PDEs are non-conservative because of the $\tau\,\partial_x(.)$ operator, the fact that $\partial_t\,\tau = 0$ in the acoustic subsystem of the current splitting and the piecewise continuous structure of the computed solution at time t^n allow to derive exactly relations (15)*. This, is a key point to make sure that the discrete acoustic relaxation subsystem is conservative which, for the present IMEX scheme, is a necessary condition to ensure that the overall fractional step approach is conservative (see* ***Proposition 1*** *below). Finally, it has to be mentioned that, up to the Mach-sensitive parameter, similar equations have already been obtained in the framework of the Lagrange-Projection methods where a mass variable m such as $\partial_m = \tau\,\partial_x$ is at stake. See [11, 8] for more details.*

The end of the scheme derivation follows naturally by remembering that W (respectively R) is constant over the 2,3 and 4-waves (respectively the 1 and 2,3-waves). Indeed, the signs of the different eigenvalues drawn on Figure 1 suggest that $W_{i+1/2}(t^n,\, t^{n+})$ (respectively $R_{i+1/2}(t^n,\, t^{n+})$) can be approximated by W_{i+1}^{n+} (respectively by R_{i-1}^{n+}). Finally the two discrete dynamics write:

$$\begin{aligned}
&\frac{W_i^{n+} - W_i^n}{\Delta t} - \frac{\left(1 - (\mathscr{E}_0^n)^2\right)\,(a_{\mathcal{A}})^n\,\tau_i^n}{\Delta x}\,\Big(W_{i+1}^{n+} - W_i^{n+}\Big) = 0,\\
&\frac{R_i^{n+} - R_i^n}{\Delta t} + \frac{\left(1 - (\mathscr{E}_0^n)^2\right)\,(a_{\mathcal{A}})^n\,\tau_i^n}{\Delta x}\,\Big(R_i^{n+} - R_{i-1}^{n+}\Big) = 0.
\end{aligned} \tag{17}$$

Thus, $\left(W_i^{n+}\right)_{i\in[1,\,N_{cells}]}$ (respectively $\left(R_i^{n+}\right)_{i\in[1,\,N_{cells}]}$) is solution of an uncoupled linear system involving an upper-bidiagonal matrix (respectively a lower-bidiagonal matrix). If transmissive boundary conditions are used by introducing fictitious states $\underline{\mathbf{U}}_0^{n+} = \underline{\mathbf{U}}_1^{n+}$ and $\underline{\mathbf{U}}_{N_{cells}+1}^{n+} = \underline{\mathbf{U}}_{N_{cells}}^{n+}$, then $W_{N_{cells}+1}^{n+} = W_{N_{cells}}^{n+}$ and $W_0^{n+} = W_1^{n+}$. The matrices involved in (17) are then non singular since all their diagonal terms are strictly positive.

4.2 Projection Step and Time-Implicit Acoustic Flux

Once the two uncoupled linear systems (17) have been solved, the time-implicit acoustic flux related to the subsystem $\mathcal{A}^{\mu}$ can be deduced immediately. It reads:

$$
\begin{aligned}
&\mathbf{H}^{\mu\ n+}_{\mathbf{ac}\,i+1/2} = \left(1-(\mathscr{C}_0^n)^2\right)\begin{bmatrix} 0 \\ (\Pi^*_{\mathcal{A}})^{n+}_{i+1/2} \\ (a^2_{\mathcal{A}})^n\,(u^*_{\mathcal{A}})^{n+}_{i+1/2} \\ (\Pi^*_{\mathcal{A}})^{n+}_{i+1/2}\,(u^*_{\mathcal{A}})^{n+}_{i+1/2} \end{bmatrix}, \\
&(u^*_{\mathcal{A}})^{n+}_{i+1/2} = \frac{R_i^{n+}+W_{i+1}^{n+}}{2}, \\
&(\Pi^*_{\mathcal{A}})^{n+}_{i+1/2} = \frac{(a_{\mathcal{A}})^n\left(R_i^{n+}-W_{i+1}^{n+}\right)}{2}.
\end{aligned}
\tag{18}
$$

In the present work, the projection step is performed instantaneously. Indeed, μ is forced to tend fictively towards zero such that $p = \Pi$. Particularly, the time-implicit acoustic pressure at face $i+1/2$ can be defined as: $(p^*_{\mathcal{A}})^{n+1}_{i+1/2} = (\Pi^*_{\mathcal{A}})^{n+}_{i+1/2}$. The other flux quantities remain invariant through the projection step. Finally the time-implicit scheme for the acoustic subsystem $\mathcal{A}$ writes:

$$
\begin{aligned}
&\mathbf{U}_i^{n+1} = \mathbf{U}_i^n - \frac{\Delta t}{\Delta x}\left(\mathbf{H}_{\mathbf{ac}}{}^{n+1}_{i+1/2} - \mathbf{H}_{\mathbf{ac}}{}^{n+1}_{i-1/2}\right), \\
&\text{with: } \mathbf{U}_i^{\sharp} = \left[\rho_i^{\sharp},\,(\rho\,u)_i^{\sharp},\,(\rho\,e)_i^{\sharp}\right]^T,\ \sharp \in \{n,\,n+1\}, \\
&\text{and: } \mathbf{H}_{\mathbf{ac}}{}^{n+1}_{i+1/2} = \left(1-(\mathscr{C}_0^n)^2\right)\begin{bmatrix} 0 \\ (p^*_{\mathcal{A}})^{n+1}_{i+1/2} \\ (p^*_{\mathcal{A}})^{n+1}_{i+1/2}\,(u^*_{\mathcal{A}})^{n+1}_{i+1/2} \end{bmatrix}.
\end{aligned}
\tag{19}
$$

It requires no particular linear solver since the two uncoupled systems (17) can be inverted by hand. Besides, as proved in Appendix A, solving the discrete momentum equation of (19) is equivalent to setting:

$$
u_i^{n+1} = \frac{R_i^{n+1}+W_i^{n+1}}{2}, \tag{20}
$$

provided that $u_i^n = \dfrac{R_i^n+W_i^n}{2}$.

In the sequel, some additional properties of the overall IMEX fractional step are presented.

4.3 The IMEX Scheme Properties

Three properties are underlined below. The two first deal with the conservativity and the maximum principle whereas the last one concerns the discrete preservation of the Riemann Invariants of single contact discontinuities.

Proposition 1. *Conservativity and maximum principle of the overall IMEX scheme:*

- *Conservativity:*

Let us formally introduce $\mathbf{H}_{\mathbf{c}}{}^n_{i+1/2}\left(\mathbf{U}_i^n,\,\mathbf{U}_{i+1}^n\right)$ *the time-explicit numerical flux associated to the subsystem* $\mathcal{C}$ *(see [23] or* (45) *in Appendix A for a definition). Then, the overall IMEX scheme is conservative and writes:*

$$
\mathbf{U}_i^{n+1} = \mathbf{U}_i^n - \frac{\Delta t}{\Delta x}\left(\mathbf{H}_{\mathbf{c}}{}^n_{i+1/2}\left(\mathbf{U}_i^n,\,\mathbf{U}_{i+1}^n\right) + \mathbf{H}_{\mathbf{ac}}{}^{n+1}_{i+1/2} - \mathbf{H}_{\mathbf{c}}{}^n_{i-1/2}\left(\mathbf{U}_{i-1}^n,\,\mathbf{U}_i^n\right) - \mathbf{H}_{\mathbf{ac}}{}^{n+1}_{i-1/2}\right). \tag{21}
$$

• *Maximum principle: Consider $\rho\,\phi$ a given conservative variable such as $\forall\,(x,\,t):\ \partial_t\,(\rho\,\phi)+\partial_x\,(\rho\,\phi\,u)=0$. Assume that $(\rho\,\phi)_i^n\in[(\rho\,\phi)_{Min},\,(\rho\,\phi)_{Max}]$. Then, the maximum principle preservation $(\rho\,\phi)_i^{n+1}\in[(\rho\,\phi)_{Min},\,(\rho\,\phi)_{Max}]$ depends only on the convective sub-step discretization. It naturally holds under a non-restrictive sufficient condition written in [23]: p.20,* ***Lemma 1 (Positivity of intermediate density)*** *] .*

It is well known that the above global conservativity result, which in this case is directly obtained because the acoustic sub-step discretization is conservative by construction, is a necessary step in order to capture the Euler physical shock fronts (see [22]). As for the maximum principle preservation for purely convected quantities, it can be considered as a first step towards the L^∞ stability of the overall scheme.

Proposition 2. *Discrete preservation of the contact discontinuity Riemann invariants:*
Assume that the equation of state is such that $(\rho\,\varepsilon)^{EOS}\,(\rho,\,p)=C(p)\,\rho+B(p)$, with $p\to C(p)$ and $p\to B(p)$ smooth functions such as $(\rho\,\varepsilon)^{EOS}_{|\rho}:\ p\to C(p)\,\rho+B(p)$ is injective on the domain of definition of p (see[16] or Appendix A for an explanation of such hypothesis); then, the overall IMEX scheme exactly preserves the constant velocity and the constant pressure of an isolated contact discontinuity from one time step to another.

According to [16], the above general expression of $(\rho\,\varepsilon)^{EOS}\,(\rho,\,p)$ belongs to the category of the "T1" equation of state. One can notably notice that the stiffened gas EOS: $\rho\,\varepsilon=p+\gamma\,\Pi$, is included in it. However the Van der Waals EOS: $\rho\,\varepsilon=\dfrac{(p+a\,\rho^2)\,(1-b\,\rho)}{\gamma-1}-a\,\rho^2$ is out of it. The above proposition will be useful in the sequel to detect the appearance of instabilities related to high convective Courant number $\mathscr{C}_{|u|}$. Proofs, including a brief description of the time-explicit convective flux related to subsystem $\mathcal{C}$, can be found in Appendix A. The next subsection is devoted to the discrete time step specification.

4.4 Construction of the Numerical time step

For a given convective Courant number $\mathscr{C}_{|u|}$, the time step at the n-th iteration of the numerical scheme is:

$$\Delta t^n=\mathscr{C}_{|u|}\frac{\Delta x}{\max\limits_i\,(|u_i^n|)}. \tag{22}$$

One should notice that the above time step formula does not take into account the real eigenvalues $u\pm\mathscr{E}_0\,c_{\mathcal{C}}$ associated to the convective subsystem $\mathcal{C}$. Besides, as described in [23], this subsystem is solved using the same relaxation techniques than these described in Section 3; the eigenvalues of the relaxation convective subsystem $\mathcal{C}^\mu$ being $u\pm\mathscr{E}_0\,a_{\mathcal{C}}\,\tau$, with $a_{\mathcal{C}}>\rho\,c_{\mathcal{C}}$. Thus, a more suitable way to set the time step in order to preserve the stability criteria of the subsystem $\mathcal{C}^\mu$ is:

$$\begin{aligned}&\Delta t_{\mathcal{C}}^n=\mathscr{C}_{\mathcal{C}}\frac{\Delta x}{\max\limits_{i+1/2}\left(max\left(\left|u_i^n-\mathscr{E}_0^n\,(a_{\mathcal{C}})_{i+1/2}^n\,\tau_i^n\right|,\,\left|u_{i+1}^n+\mathscr{E}_0^n\,(a_{\mathcal{C}})_{i+1/2}^n\,\tau_{i+1}^n\right|\right)\right)},\\&(a_{\mathcal{C}}^n)_{i+1/2}=K\,max\,(\rho_i^n\,(c_{\mathcal{C}})_i^n,\,\rho_{i+1}^n\,(c_{\mathcal{C}})_{i+1}^n)\,,\ K>1.\end{aligned} \tag{23}$$

In practice, formula (22) is implemented because, contrary to (23), it does not contain any dependence in the speed of sound. Nevertheless, in Section 6, the influence of the choice of Δt^n rather than Δt^n_C can be seen through a stability analysis.

The following section is devoted to one-dimensional numerical results produced by the present IMEX approach.

5 Numerical Results

5.1 Low Mach Isolated Waves

The first part of the numerical results is dedicated to the influence of the Courant number on quantities varying through the acoustic or material waves. Indeed, it is well known (see [27, 28, 2, 3, 26, 12]) that time-implicit schemes, even if of high order in space, are only accurate on σ-like waves when the time steps Δt are such that $\mathscr{C}_\sigma = (|\sigma|\ \Delta t)/\Delta x \approx 1$. In the following, one seeks to investigate the accuracy of the above IMEX fractional step with respect to $\mathscr{C}_{|u|}$ and compare it with an other IMEX Lagrange-Projection (LP) fractional step described in [8, 7] in the context of low Mach number flows. Two low Mach number cases are thus evaluated. The first one details the propagation of a single 3-shock wave while the second one corresponds to the evolution of a single contact wave. In both cases, particular attention will be paid to the diffusive or stiffening effects associated to the increase of $\mathscr{C}_{|u|}$.

5.1.1 Isolated Shock Wave

For this test case, the fluid is endowed with a perfect gas thermodynamics $\varepsilon = p/\left((\gamma-1)\,\rho\right)$, and $c = \sqrt{\gamma\, p/\rho}$ with $\gamma = 7/5$, the heat capacity ratio. The left state of the considered 3-isolated shock wave is completely defined by $\rho^0_L = 1\ (kg.m^{-3})$, $p^0_L = 10^4\ (Pa)$ and $u^0_L = M_0 \times c^0_L$ with $M_0 = 10^{-2}$ the maximal Mach number of the flow. Besides, the shock wave speed σ is fixed equal to $c^0_L \approx 118.32\ (m.s^{-1})$. The three remaining unknowns ρ^0_R, u^0_R and p^0_R are the solutions of the corresponding Rankine-Hugoniot problem and can then be found analytically. Besides, the resulting right state abides by the Lax entropy criterion: $u^0_R + c^0_R < \sigma < u^0_L + c^0_L$.

On Figure 2, the isolated 3-shock wave pressure profile is shown. The physical time of the simulation is such that the initial discontinuity located at $x_0 = 0.5\ m$ stops at $x = 0.75\ m$. The mesh is made of 10^3 cells. Different curves are plotted; Sp-(M) stands for the current splitting presented in (2) and (3) whereas Sp-LP refers to a Lagrange-Projection splitting method fully described in [8] and taken as a benchmark in this work. Besides the abbreviation "Exp" indicates that the acoustic part of the Sp-(M) splitting (respectively the Sp-LP splitting) has been discretized using a time-explicit scheme detailed in [23] (respectively [8]). In this case, the CFL condition is such that $\mathscr{C}_E = 1$. On the contrary "Imp" refers to the above time-implicit approach.

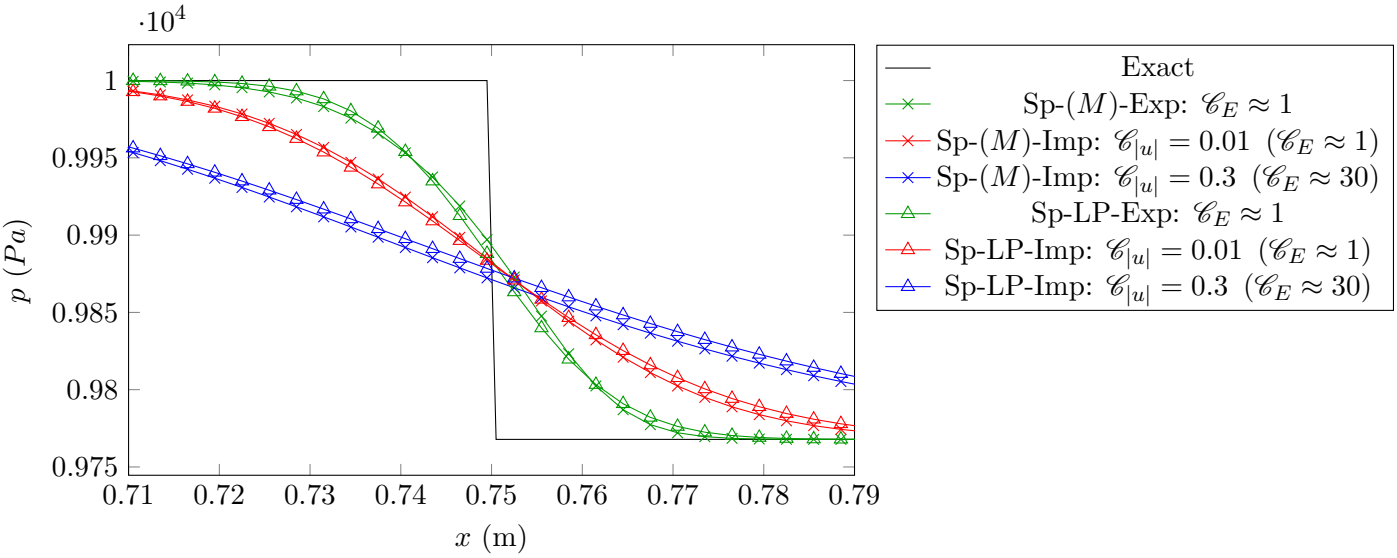

Figure 2: Pressure profile, Perfect Gas, $M = 10^{-2}$, with $N_{cells} = 10^3$

Two different convective Courant numbers values have been tested in the implicit-explicit approaches: the first one $\mathscr{C}_{|u|} = 0.01$ has been deliberately chosen to provide time steps close to those based on the constraint $\mathscr{C}_E \approx 1$ since formally $\mathscr{C}_{|u|} = M/(1+M)\mathscr{C}_E$ and $M = 10^{-2}$. The other value $\mathscr{C}_{|u|} = 0.3$ corresponds to $\mathscr{C}_E \approx 30$ and is thus expected to be too high for the IMEX scheme to accurately follow the shock wave front.

It turns out that, in this low Mach number case, the sharper pressure profiles are those provided by the time-explicit schemes complying with the constraint: $\mathscr{C}_E \approx 1$. On the contrary the closer to one is $\mathscr{C}_{|u|}$, the more diffused the shock profile is. Besides, for a fixed Euler Courant number $\mathscr{C}_E \approx 1$, the averaging effect of the time-implicit schemes relatively to the time-explicit ones can be observed as the profile of "Sp-(M)-Imp: $\mathscr{C}_{|u|} = 0.01$" is largely more diffused than "Sp-(M)-Exp: $\mathscr{C}_E = 1$". Finally, one can notice that, for all the Courant number values involved here, the Sp-(M) splitting is as accurate as the Sp-LP method. These results, obtained in the context of the Euler system, seem to be close to the predictions given by the linear stability analysis in [12].

This simple test case, involving a fast acoustic wave related to a genuinely non-linear field, has allowed to test the robustness with respect to $\mathscr{C}_{|u|}$ of the present approach compared to the LP method. In the sequel the same study is performed on a slow material wave associated with a linearly degenerate field.

5.1.2 Isolated Contact Discontinuity

For the same thermodynamical law, a single contact discontinuity is created by imposing: $\rho_L^0 = 1$ $(kg.m^{-3})$, $\rho_R^0 = 0.125$ $(kg.m^{-3})$, $p_L^0 = p_R^0 = p^0 = 10^4$ (Pa), $u_L^0 = u_R^0 = M_0 \times c_R^0 = u^0$ with $M_0 = 10^{-2}$. This wave linked to a linear degenerate field propagates at speed $u_0 \approx 3.35$ $(m.s^{-1})$.

On Figure 3, one can observe the density profiles. As it was expected, the isolated contact discontinuity sharpens as the convective Courant number $\mathscr{C}_{|u|}$ reaches 1. Once again, for the same Courant number,

the profiles between the present IMEX scheme and the IMEX-LP scheme overlap quasi-perfectly.

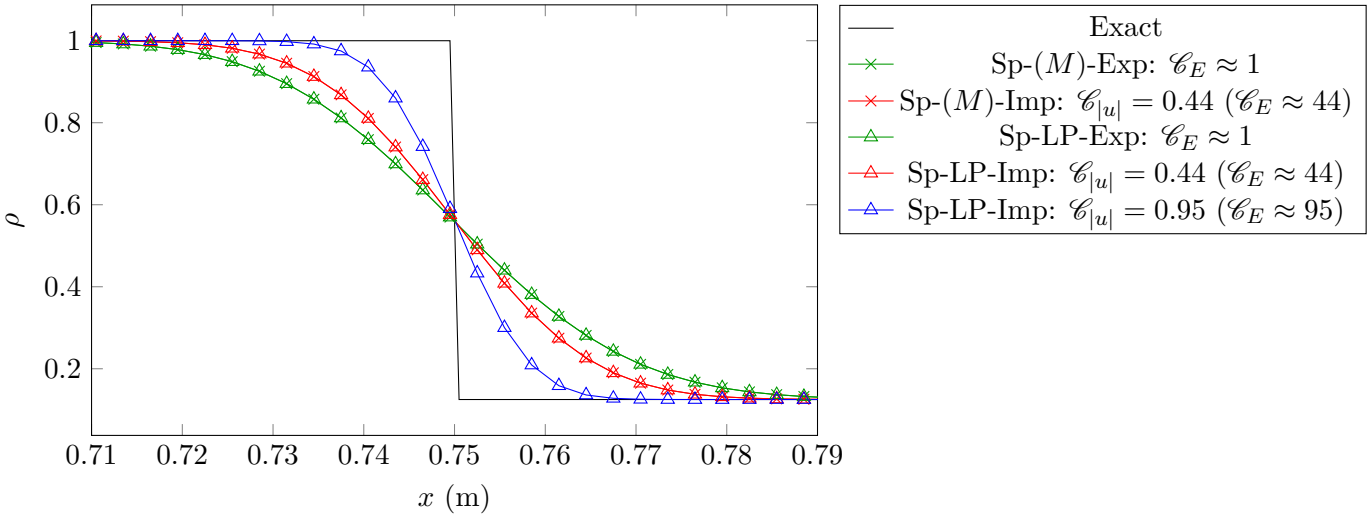

Figure 3: Density profile, Perfect Gas, $M_{min} = 10^{-2}$, with $N_{cells} = 10^3$

However, one can notice that the ideal target associated to $\mathscr{C}_{|u|} = 0.95 \approx 1$ has only been achieved for the LP method. Indeed, for this test case, the present splitting and the resulting IMEX approach triggers instabilities for $\mathscr{C}_{|u|}$ above 0.44. A tentative of explanation for this stability issue is done further in Section 6.

In the sequel, accuracy and efficiency of the above IMEX schemes are compared to their full time-explicit versions in the context of low Mach number flows.

5.2 A Low Mach Sod Shock Tube

After having measured the impact of the IMEX fractional step approach on isolated waves, one wishes to extend the study to multiple waves test cases. Herein, a low Mach number shock tube is computed. The fluid is endowed with the same previous perfect gas thermodynamics. The initial conditions are made of a density discontinuity $\rho_L^0 = 1\ kg\,m^{-3}$, $\rho_L^0 = 0.125\ kg\,m^{-3}$, a constant velocity $u_L^0 = u_R^0 = u^0 = 1\ m\,s^{-1}$, and a slightly discontinuous pressure $p_L^0 = 10080\ Pa$, $p_R^0 = 10000\ Pa$. It results in a left-going 1-rarefaction wave, a 2-contact discontinuity propagating to the right and a right-going 3-shock wave. The maximal Mach number of the flow, reached in the head of the rarefaction wave, is equal to 1.26×10^{-2}.

Various time-explicit schemes have been tested: "no-Sp" corresponds to the case where $\mathscr{E}_0^n = 1$ is imposed along the simulation. Thus, the splitting is not triggered. "Sp-($\sqrt{M}$)" is the weighted splitting approach with $\mathscr{E}_0^n = \max\left(\sqrt{M_{inf}}, \min\left(\sqrt{M_{max}^n}, 1\right)\right)$ while "Sp-(M)" involves $\mathscr{E}_0^n$ defined in formula (16) which is *a priori* optimal for a time-explicit scheme, because, as shown in [23], it minimizes the numerical diffusion of the subsystem $\mathcal{C}$ in the low-Mach number case. Lastly, "Sp-LP" is again the Lagrange Projection splitting method, described in [8]. Besides, the mention "-corr" means that a low-Mach correction inspired from [14] and written in [23] is triggered. As observed in [23, 8, 7], it

aims at considerably reducing the numerical diffusion in the case of low Mach number flows.

Regarding the time-implicit schemes, two values for $\mathscr{C}_{|u|}$ have been tested. As shown in Appendix D, the ratio between $\mathscr{C}_{|u|}$ the convective Courant number based on u^0 and $\mathscr{C}_E^{0,*}$ the most constraining Euler Courant number is:

$$\mathscr{C}_{|u|}^{u^0} \approx 1.5 \times 10^{-3}\, \mathscr{C}_E^{0,*}. \tag{24}$$

Then, the selected convective Courant numbers are $\mathscr{C}_{|u|} = 1.5 \times 10^{-2}$ ($\mathscr{C}_E^{0,*} \approx 10$) and $\mathscr{C}_{|u|} = 4.5 \times 10^{-2}$ ($\mathscr{C}_E^{0,*} \approx 30$).

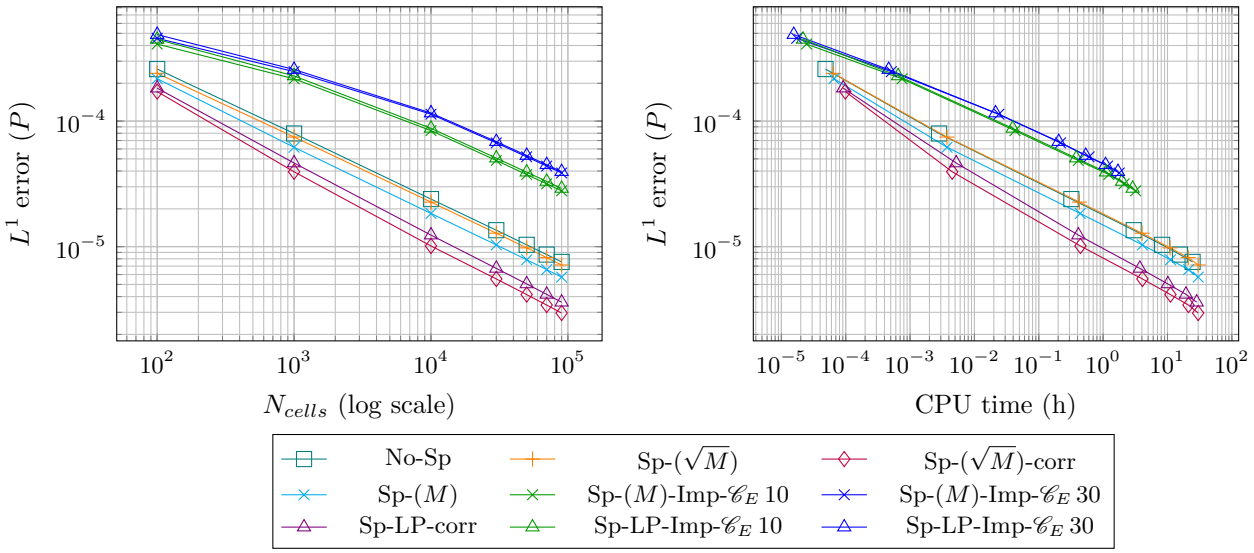

Figure 4: P Convergence Curve (left), Efficiency Curve (right): $M = 1.26 \times 10^{-2}$

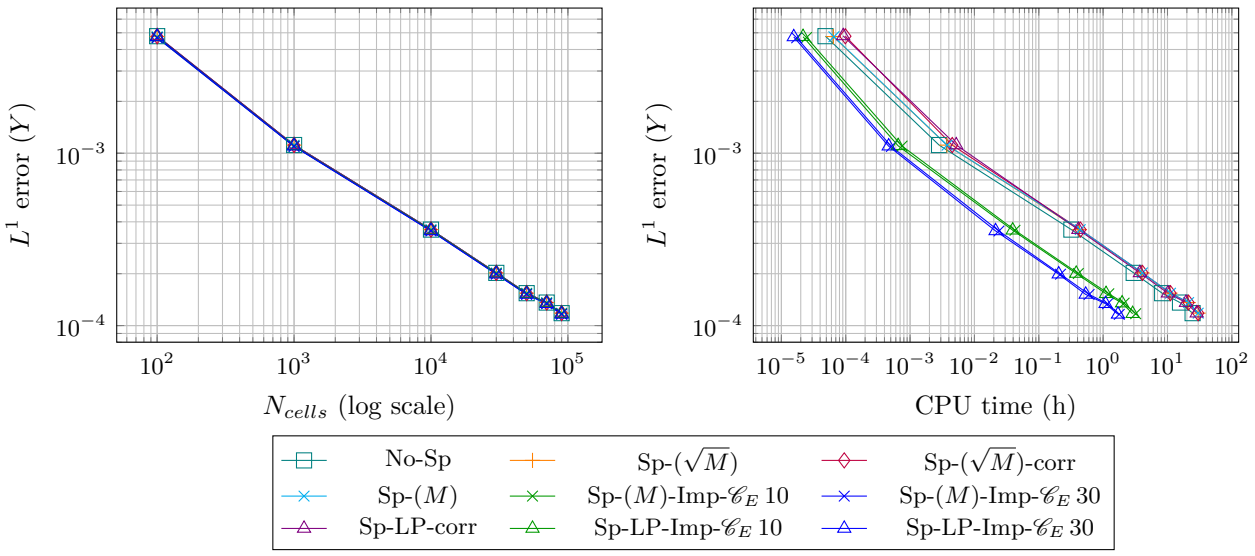

Figure 5: Y Convergence Curve (left), Efficiency Curve (right): $M = 1.26 \times 10^{-2}$

In this test case, in order to isolate the effect of the IMEX scheme on the contact discontinuity, a passive tracer Y has been added to the Euler system. Its PDE being:

$$\partial_t (\rho Y) + \partial_x (\rho Y u) = 0. \tag{25}$$

Starting from $Y_L^0 = 1$ and $Y_R^0 = 0.5$, the exact solution jumps only through the contact discontinuity.

Figure 4 (respectively Figure 5) presents the convergence curve and the efficiency curve for the pressure (respectively Y) variable. As already pointed out in [23], for such a low Mach number, and focusing on the pressure (or any variable jumping through the genuinely non-linear fields), the time-explicit schemes with the low Mach number correction Sp-($\sqrt{M}$)-corr and Sp-LP-corr, are the most accurate as well as the most efficient. As already observed in the isolated 3-shock wave test case, time-implicit schemes such that $\mathscr{C}_E > 1$ are less accurate than any of the time-explicit schemes. Besides, according to the pressure efficiency curve, this lack of accuracy is not compensated by a substantial gain in CPU time. Indeed, for a given pressure L^1-error level, time-implicit schemes are still more CPU-consuming than the time-explicit ones.

In the case of the passive tracer Y, no specific difference on the convergence curve can be noticed between the time-explicit and the time-implicit schemes. Indeed, the convective Courant number $\mathscr{C}_{|u|} \leq 3 \times 10^{-2}$ is still very far from one. Thus for every scheme, numerical diffusion has uniformly smoothed the variables only jumping through the slow material wave. Nevertheless, as shown on Table 1, time-implicit schemes are clearly more efficient, for the Y variable, than the time-explicit ones, the latter being 7 (respectively 13) times more CPU-consuming than time-implicit schemes when setting $\mathscr{C}_E^{0,*} = 10$ (respectively $\mathscr{C}_E^{0,*} = 30$).

$Ncells$	$\mathscr{C}_E = 10$	$\mathscr{C}_E = 30$
10^2	1.97	2.80
10^3	3.75	5.51
10^4	7.52	13.36
3×10^4	7.26	13.71
5×10^4	6.74	13.66
7×10^4	7.39	13.34
9×10^4	7.67	13.78

Table 1: $T^{\text{CPU}}_{\text{No-Sp}}/T^{\text{CPU}}_{\text{Sp-}(M)\text{-Imp}}$

The next section is a sketch of stability analysis in order to determine an upper bound for the convective Courant number under which the present IMEX scheme remains stable.

6 Stability Analysis

Let us consider the isolated contact discontinuity test case with a 10^3 cells mesh discussed in sub-section 5.1.2. As shown on Figure 8 and Figure 9 in Appendix C, the present splitting seems to suffer from instabilities when the convective Courant number $\mathscr{C}_{|u|}$ goes over a certain threshold. In the following the dependence to the Mach number M of such a threshold is examined. Among other questions, one wonders whether the time-explicit CFL condition $\mathscr{C}_{|u|} = M/(1+M)$ is retrieved as M tends toward zero?

As stated in **Proposition** 2 for a sufficiently simple shape of the equation of state, velocity and pressure are supposed to be left constant by the overall scheme from one time step to another. Nonetheless, truncation errors on double-precision floating-point numbers can be amplified by the scheme's instability and lead to the crash of the simulation. Thus, the selected criterion to detect the instability appearance is: $\max_i \left(\left| p_i^n - p^0 \right| \right) / p^0 > \eta$ with $\eta = 10^{-7}$ which is nearly the single-precision for floating-point numbers. Besides at the beginning of each calculation a ramp of CFL is enforced so that the targeted Courant number is reached after 200 time steps, which corresponds to a propagation of 0.1 m of the exact contact discontinuity. If the calculation ends without triggering the above pressure stability criterion then the same calculation is launched again on a five times finer mesh of 5×10^3 cells in order to make sure that the numerical diffusion has not damped the instability appearance.

On Figure 6, the curve labeled Sp-(M) gathers the different points resulting from the above stable convective Courant number research. Recall that in this test case the velocity is given by $u^0 = M_{min}\, c_R^0$, with $c^{0,R} = \sqrt{(\gamma\, p^0)/\rho_R^0}$ the maximal sound speed and M_{min} the minimal Mach number of the flow used as an input parameter here. Hence the stable Courant number upper bound is displayed as a function of M_{min}. The latter starts from $M_{min} = 1,\ u^0 = 335\,(m.s^{-1})$ and decreases until $M_{min} = 10^{-4},\ u^0 = 0.0335\,(m.s^{-1})$.

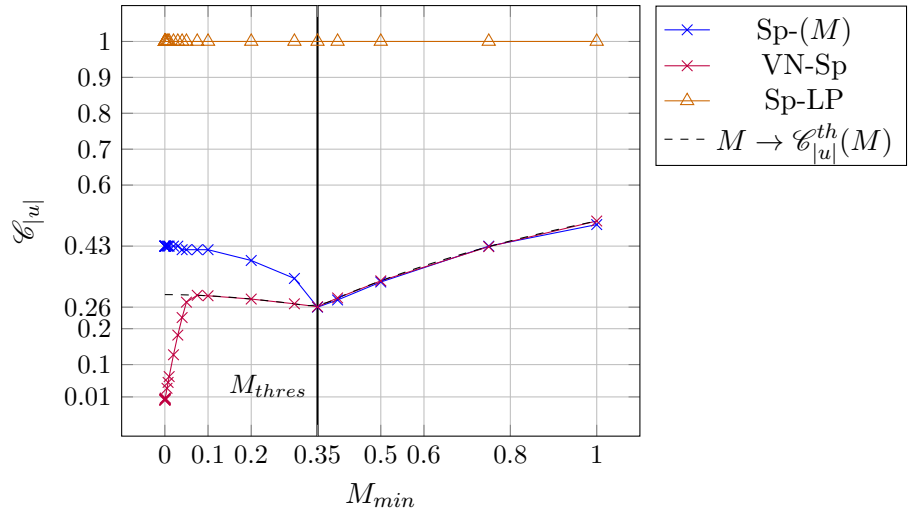

Figure 6: Evaluation of an upper bound for the stable convective Courant number $\mathscr{C}_{|u|}$ as function of the Mach number M_{min}

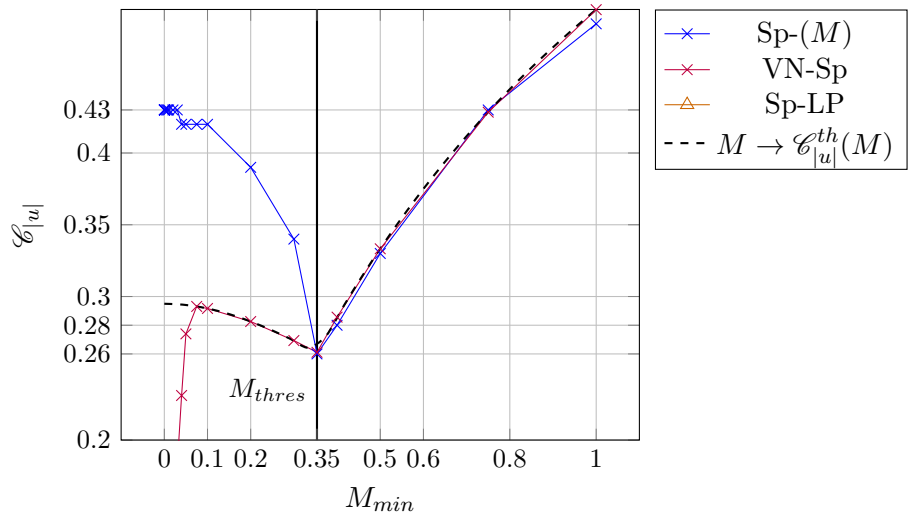

Figure 7: Evaluation of an upper bound for the stable convective Courant number $\mathscr{C}_{|u|}$ as function of the Mach number M_{min}, $\mathscr{C}_{|u|} \in [0.2,\, 0.5]$

One can observe that for $M_{min} \approx 1$, $\mathscr{E}_0^n \approx 1$ so that the full Euler system is brought back into the time-explicit convective subsystem. The latter is thus bound by the classical CFL condition $\mathscr{C}_E \approx 0.49$. Then, as the Mach number decreases, the contribution of the acoustic subsystem becomes more and more effective. It results in a drop of the Euler time-explicit CFL condition until $M_{min} \approx 0.35$ where $\mathscr{C}_{|u|} = 0.26$. This decline might be related to the gap between the definition of $\mathscr{C}_{|u|}$ and the Courant number involving the biggest eigenvalues of the convective subsystem:

$$\mathscr{C}_{\mathcal{C}} = \frac{\left(\left|u^0\right| + \mathscr{E}_0^n \, c_{\mathcal{C}}^{0,\,R}\right) \Delta t}{\Delta x}, \quad \text{with: } c_{\mathcal{C}}^{0,\,R} = c_{\mathcal{C}}\left(\rho_R^0,\, p^0\right). \tag{26}$$

One can notice that:

$$\begin{aligned} &\mathscr{C}_{|u|} = \left(1 + \mathscr{E}_0^n \, \frac{c_{\mathcal{C}}^{0,\,R}}{|u^0|}\right)^{-1} \mathscr{C}_{\mathcal{C}} = \left(1 + \frac{\mathscr{E}_0^n}{M_{min}} \, \frac{c_{\mathcal{C}}^{0,\,R}}{c^{0,\,R}}\right)^{-1} \mathscr{C}_{\mathcal{C}}, \\ &\text{since: } \left|u^0\right| = M_{min} \, c^{0,\,R}, \\ &\text{and: } \frac{c_{\mathcal{C}}^{0,\,R}}{c^{0,\,R}} = \sqrt{(\mathscr{E}_0^n)^2 \frac{\gamma - 1}{\gamma} + \frac{1}{\gamma}} \in [1/\gamma,\, 1]\,. \end{aligned} \tag{27}$$

Besides, according to formula (16):

$$\begin{aligned} \mathscr{E}_0^n = \min\left(M_{max}^n,\, 1\right) &= \min\left(\left|u^0\right| / c^{0,\,L},\, 1\right) \\ &= \min\left(M_{min} \sqrt{\frac{\rho_L^0}{\rho_R^0}},\, 1\right), \\ \text{then } \forall M_{min} \geq M_{thres} = \sqrt{\frac{\rho_R^0}{\rho_L^0}} &: \;\; \mathscr{E}_0^n = 1, \\ \text{and } \forall M_{min} < M_{thres} = \sqrt{\frac{\rho_R^0}{\rho_L^0}} &: \;\; \mathscr{E}_0^n = M_{min}/M_{thres}. \end{aligned} \tag{28}$$

It results that:

$$\mathscr{C}_{|u|} = \begin{cases} \left(1 + \dfrac{1}{M_{min}}\right)^{-1} \mathscr{C}_{\mathcal{C}}, & \text{if: } M_{min} \geq M_{thres}, \\ \left(1 + \dfrac{1}{M_{thres}} \sqrt{\left(\dfrac{M_{min}}{M_{thres}}\right)^2 \dfrac{\gamma - 1}{\gamma} + \dfrac{1}{\gamma}}\right)^{-1} \mathscr{C}_{\mathcal{C}}, & \text{otherwise.} \end{cases} \tag{29}$$

Define $M_{min} \rightarrow \mathscr{C}_{|u|}^{th}(M_{min})$, the continuous function described by formula (29). This function has been plotted as a dashed black line on Figure 6 and Figure 7. Then, one can notice that when $M_{min} = 1$, $\mathscr{C}_{|u|}^{th}(M_{min}) = \mathscr{C}_{\mathcal{C}}/2$ whereas it reaches a plateau value $\left(1 + \dfrac{1}{M_{thres}\sqrt{\gamma}}\right)^{-1}$ as M_{min} tends towards zero. If one assumes that the time-explicit scheme associated to the convective subsystem is stable for $\mathscr{C}_{\mathcal{C}} \approx 1$, then one finds numerically that $\mathscr{C}_{|u|}^{th}(1) \approx 0.5$ while $\lim\limits_{M_{min} \rightarrow 0} \mathscr{C}_{|u|}^{th}(M_{min}) \approx 0.2949$. Besides, $M_{thres} \approx 0.3535$ and $\mathscr{C}_{|u|}^{th}(M_{thres}) \approx 0.2612$. Actually, for every M_{min} between M_{thres} and 1 the comparison between $\mathscr{C}_{|u|}^{th}$ and the measured stable convective Courant number is fair: the cut-off $M_{min} = M_{thres}$, the $\mathscr{C}_{|u|}^{th}(M_{thres})$ value as well as the global shape of $\mathscr{C}_{|u|}^{th}(.)$ are retrieved. Yet, as M_{min} falls below M_{thres}, the measured stable convective Courant number increases to reach the plateau value

$\mathscr{C}_{|u|} = 0.43$ which is bigger than the one predicted by the above analysis. Nevertheless it seems that, on this test case, $\mathscr{C}_{|u|} \approx 0.3$ is sufficient to ensure the scheme stability for *every Mach number*. According to Zakerzadeh in [36], this is what is called the "Mach-uniform" stability property. This latter result is absolutely not guaranteed by the time-implicit integration of the stiff part of the IMEX approach and strongly depends on the splitting at stake. Indeed, in [31, 37] several IMEX fractional steps on Euler-like systems are studied. It turns out that the "modified" equation obtained from the order two Taylor expansion of a smooth solution of an IMEX fractional step approach exhibits a diffusive operator which can be written $\mathbf{D}_0\,\partial_{xx}\,\mathbf{U}$; with $\mathbf{D}_0 = \beta\,\mathscr{C}_{|u|}\,\mathbf{I} - (\mathbf{A}_0^{\mathcal{C}})^2 + (\mathbf{A}_0^{\mathcal{A}})^2 + \left[\mathbf{A}_0^{\mathcal{C}},\,\mathbf{A}_0^{\mathcal{A}}\right]$, β being a coefficient related to the scheme numerical diffusion of the convective sub-step, $\mathbf{A}_0^{\mathcal{C}}$ (respectively $\mathbf{A}_0^{\mathcal{A}}$) the linearized jacobian matrix related to the convective (respectively the acoustic) subsystem, and $\left[\mathbf{A}_0^{\mathcal{C}},\,\mathbf{A}_0^{\mathcal{A}}\right] = \mathbf{A}_0^{\mathcal{C}}\,\mathbf{A}_0^{\mathcal{A}} - \mathbf{A}_0^{\mathcal{A}}\,\mathbf{A}_0^{\mathcal{C}}$ being the commutator linked to the splitting. The latter can be viewed as a mathematical operator which couples the two subsystems of the fractional step approach. Hence, even if it is discretized using a time-implicit scheme, the acoustic subsystem can still have an influence on the overall fractional step stability through the commutator which can impact the diffusion (or the anti-diffusion) effect of the modified equation. On Figure 6, the orange-triangle line labeled "Sp-LP" represents the stable convective Courant number obtained with the Lagrange-Projection IMEX approach. As already proven in [36], this scheme is Mach-uniformly stable for $\mathscr{C}_{|u|} = 1$.

In order to better understand the shape of the stable Courant number, a von Neumann-like stability analysis based on a linearized version of the IMEX approach has been performed. This strategy is motivated by the fact that, as shown on Figure 8 of Appendix C, the instability seems to appear in a region where ρ, u and p are constant. The linearization required by the von Neumann analysis is thus justified. However, one should keep in mind that such a method relies on periodic boundary conditions which is not the case here because of the density discontinuity.

Starting at time step t^n with a perturbed constant flow:

$$\begin{aligned} \rho_i^n &= \rho^0 + \epsilon\,\rho_i^{1,\,n},\ \rho^0 = \rho_R^0, \\ u_i^n &= u^0 + \epsilon\,u_i^{1,\,n}, \\ p_i^n &= p^0 + \epsilon\,p_i^{1,\,n}, \end{aligned} \tag{30}$$

the discrete dynamics of the perturbation is derived when a Rusanov scheme is used to solve the first convective subsystem (2). The numerical flux at face $i+1/2$ associated to this scheme reads:

$$\begin{aligned} &\mathbf{H_{rus}}_{i+1/2}^{n} = \frac{\mathbf{F}^{\mathcal{C}}\left(\mathbf{U}_{i+1}^n\right) + \mathbf{F}^{\mathcal{C}}\left(\mathbf{U}_i^n\right)}{2} - \frac{\left|\lambda_{i+1/2}^n\right|}{2}\left(\mathbf{U}_{i+1}^n - \mathbf{U}_i^n\right), \\ &\text{with: } \mathbf{F}^{\mathcal{C}}\left(\mathbf{U}\right) = \left[\rho\,u,\,\rho\,u^2 + \mathscr{E}_0^2\,p,\,\left(\rho\,e + \mathscr{E}_0^2\,p\right)u\right]^T, \\ &\text{and: } \left|\lambda_{i+1/2}^n\right| = \max\left(|u_{i+1}^n| + (\mathscr{E}_0)^n\,(c_{\mathcal{C}})_{i+1}^n,\,|u_i^n| + (\mathscr{E}_0)^n\,(c_{\mathcal{C}})_i^n\right). \end{aligned} \tag{31}$$

Let us define $\rho_i^{n+} = \rho_i^{0,\,n+} + \epsilon\,\rho_i^{1,\,n+}$, $u_i^{n+} = u_i^{0,\,n+} + \epsilon\,u_i^{1,\,n+}$, and $p_i^{n+} = p_i^{0,\,n+} + \epsilon\,p_i^{1,\,n+}$ the solution produced by the Rusanov scheme applied to the convective subsystem. Then, zeroth order and first order dynamics can be decoupled and one obtains:

$$
\begin{aligned}
&\rho_i^{0,\,n+} = \rho^0,\\
&u_i^{0,\,n+} = u^0,\\
&p_i^{0,\,n+} = p^0,\\
&\frac{\rho_i^{1,\,n+} - \rho_i^{1,\,n}}{\Delta t} + u^0\,\frac{\rho_{i+1}^{1,\,n} - \rho_{i-1}^{1,\,n}}{2\,\Delta x} + \rho^0\,\frac{u_{i+1}^{1,\,n} - u_{i-1}^{1,\,n}}{2\,\Delta x} - \left|\lambda^0\right|\,\frac{\rho_{i+1}^{1,\,n} - 2\,\rho_i^{1,\,n} + \rho_{i-1}^{1,\,n}}{2\,\Delta x} = 0,\\
&\frac{u_i^{1,\,n+} - u_i^{1,\,n}}{\Delta t} + u^0\,\frac{u_{i+1}^{1,\,n} - u_{i-1}^{1,\,n}}{2\,\Delta x} + \left((\mathscr{E}_0^n)^2/\rho^0\right)\,\frac{p_{i+1}^{1,\,n} - p_{i-1}^{1,\,n}}{2\,\Delta x} - \left|\lambda^0\right|\,\frac{u_{i+1}^{1,\,n} - 2\,u_i^{1,\,n} + u_{i-1}^{1,\,n}}{2\,\Delta x} = 0,\\
&\frac{p_i^{1,\,n+} - p_i^{1,\,n}}{\Delta t} + u^0\,\frac{p_{i+1}^{1,\,n} - p_{i-1}^{1,\,n}}{2\,\Delta x} + \rho^0\,(c_{\mathcal{C}}^0)^2\,\frac{u_{i+1}^{1,\,n} - u_{i-1}^{1,\,n}}{2\,\Delta x} - \left|\lambda^0\right|\,\frac{p_{i+1}^{1,\,n} - 2\,p_i^{1,\,n} + p_{i-1}^{1,\,n}}{2\,\Delta x} = 0,\\
&\text{with: } \left|\lambda^0\right| = \left|u^0\right| + (\mathscr{E}_0)^n\,(c_{\mathcal{C}}^0).
\end{aligned}
\tag{32}
$$

If $\forall \phi \in \{\rho,\, u,\, p\}$ the following sinus spatial pulse is conjectured $\phi_i^t = \hat{\phi}^t\, e^{j\,k\,x_i},\ t \in \{n,\, n+\}$; one can derive the von Neumann gain matrix related to the convective subsystem:

$$
\begin{bmatrix} \hat{\rho}^{n+} \\ \hat{u}^{n+} \\ \hat{p}^{n+} \end{bmatrix} = \begin{bmatrix} G & -\dfrac{\rho^0\,\mathscr{C}_{|u|}}{|u^0|}\,j\,sin(k\,\Delta x) & 0 \\ 0 & G & -\dfrac{(\mathscr{E}_0^n)^2\,\mathscr{C}_{|u|}}{\rho^0\ |u^0|}\,j\,sin(k\,\Delta x) \\ 0 & -\dfrac{\rho^0\,(c_{\mathcal{C}}^0)^2\,\mathscr{C}_{|u|}}{|u^0|}\,j\,sin(k\,\Delta x) & G \end{bmatrix} \begin{bmatrix} \hat{\rho}^n \\ \hat{u}^n \\ \hat{p}^n \end{bmatrix},
$$
$$
\text{with: } G = 1 - 2\frac{\left|\lambda^0\right|}{|u^0|}\mathscr{C}_{|u|}\,sin^2(k\,\Delta x/2) - j\,\frac{u^0}{|u^0|}\mathscr{C}_{|u|}\,sin(k\,\Delta x).
\tag{33}
$$

The spectral radius $|G|_{\mathcal{C}}$ related to this gain matrix can be found easily and one can state that (See Appendix B for a proof):

$$
\mathscr{C}_{|u|} < \mathscr{C}_{|u|}^{\text{crit}} = \left|u^0\right| / \left|\lambda^0\right| \Rightarrow |G|_{\mathcal{C}} < 1. \tag{34}
$$

In particular, when M_{min} tends towards one, $(\mathscr{E}_0)^n$ tends towards one and $c_{\mathcal{C}}^0$ tends towards c^0 such that $|G|_{\mathcal{C}} < 1 \Leftrightarrow \mathscr{C}_{|u|} < M_{min}/\,(1 + M_{min})$. Thus, the classical CFL condition is retrieved.

The same kind of analysis is performed on the acoustic subsystem. However, the time-implicit flux (19) raises new issues in the sense that its energy contribution strongly couples zeroth-order and first-order terms: $(p_{\mathcal{A}}^*)_{i+1/2}^{n+1}\,(u_{\mathcal{A}}^*)_{i+1/2}^{n+1} = (p_{\mathcal{A}}^{0,\,*})_{i+1/2}^{n+1}\,(u_{\mathcal{A}}^{0,\,*})_{i+1/2}^{n+1} + \epsilon\left((p_{\mathcal{A}}^{0,\,*})_{i+1/2}^{n+1}\,(u_{\mathcal{A}}^{1,\,*})_{i+1/2}^{n+1} + (p_{\mathcal{A}}^{1,\,*})_{i+1/2}^{n+1}\,(u_{\mathcal{A}}^{0,\,*})_{i+1/2}^{n+1}\right)$. What is more, this coupling is strongly non-linear and prevents from deriving a simple von Neumann analysis. That is why, it has been additionally assumed that zeroth-order terms including these taken at time t^{n+1} were constant namely:

$$
\begin{aligned}
&\rho_i^{0,\,n+1} = \rho^0,\\
&u_i^{0,\,n+1} = u^0,\\
&p_i^{0,\,n+1} = p^0;
\end{aligned}
\tag{35}
$$

then, as proved in Appendix B the dynamics of the perturbation reads:

$$
\begin{aligned}
&\frac{\rho_i^{1,n+1}-\rho_i^{1,n+}}{\Delta t}=0,\\
&\frac{u_i^{1,n+1}-u_i^{1,n+}}{\Delta t}+\left(1-(\mathscr{E}_0^n)^2\right)\left[\frac{1}{\rho^0}\frac{p_{i+1}^{1,n+1}-p_{i-1}^{1,n+1}}{2\,\Delta x}-\frac{a_{\mathcal{A}}^0}{\rho^0}\frac{u_{i+1}^{1,n+1}-2\,u_i^{1,n+1}+u_{i-1}^{1,n+1}}{2\,\Delta x}\right]=0,\\
&\frac{p_i^{1,n+1}-p_i^{1,n+}}{\Delta t}+\left(1-(\mathscr{E}_0^n)^2\right)\rho^0\,(c_{\mathcal{A}}^0)^2\left[\frac{u_{i+1}^{1,n+1}-u_{i-1}^{1,n+1}}{2\,\Delta x}-\frac{1}{a_{\mathcal{A}}^0}\frac{p_{i+1}^{1,n+1}-2\,p_i^{1,n+1}+p_{i-1}^{1,n+1}}{2\,\Delta x}\right]=0.
\end{aligned}
\tag{36}
$$

The von Neumann gain matrix writes:

$$
\begin{aligned}
&\begin{bmatrix}1 & 0 & 0\\ 0 & 1+2\,\alpha^n\,sin^2(k\,\Delta x/2) & \dfrac{\alpha^n}{a_{\mathcal{A}}^0}j\,sin(k\,\Delta x)\\ 0 & \alpha^n\,(\omega_{\mathcal{A}}^0)^2\,a_{\mathcal{A}}^0\,j\,sin(k\,\Delta x) & 1+2\,\alpha^n(\omega_{\mathcal{A}}^0)^2\,sin^2(k\,\Delta x/2)\end{bmatrix}\begin{bmatrix}\hat{\rho}^{n+1}\\ \hat{u}^{n+1}\\ \hat{p}^{n+1}\end{bmatrix}=\begin{bmatrix}\hat{\rho}^{n+}\\ \hat{u}^{n+}\\ \hat{p}^{n+}\end{bmatrix},\\
&\text{with: } \alpha^n=\left(1-(\mathscr{E}_0^n)^2\right)\frac{a_{\mathcal{A}}^0\,\mathscr{C}_{|u|}}{\rho^0\,|u^0|},\\
&\text{and: } \omega_{\mathcal{A}}^0=\frac{\rho^0\,c_{\mathcal{A}}^0}{a_{\mathcal{A}}^0}.
\end{aligned}
\tag{37}
$$

Finally the von Neumann gain matrix related to the fractional step approach reads:

$$
\begin{aligned}
&\begin{bmatrix}G & 0\\ 0 & \mathbf{G}_{\mathcal{A}}^{-1}\,\mathbf{G}_{\mathcal{C}}\end{bmatrix},\\
&\text{with:}\\
&\mathbf{G}_{\mathcal{C}}=\begin{bmatrix}G & -\dfrac{(\mathscr{E}_0^n)^2\,\mathscr{C}_{|u|}}{\rho^0\,|u^0|}j\,sin(k\,\Delta x)\\ -\dfrac{\rho^0\,(c_{\mathcal{C}}^0)^2\,\mathscr{C}_{|u|}}{|u^0|}j\,sin(k\,\Delta x) & G\end{bmatrix},\\
&\mathbf{G}_{\mathcal{A}}=\begin{bmatrix}1+2\,\alpha^n\,sin^2(k\,\Delta x/2) & \dfrac{\alpha^n}{a_{\mathcal{A}}^0}j\,sin(k\,\Delta x)\\ \alpha^n\,(\omega_{\mathcal{A}}^0)^2\,a_{\mathcal{A}}^0\,j\,sin(k\,\Delta x) & 1+2\,\alpha^n(\omega_{\mathcal{A}}^0)^2\,sin^2(k\,\Delta x/2)\end{bmatrix},\\
&\mathbf{G}_{\mathcal{A}}^{-1}=\frac{1}{\Delta}\begin{bmatrix}1+2\,\alpha^n\,(\omega_{\mathcal{A}}^0)^2\,sin^2(k\,\Delta x/2) & -\dfrac{\alpha^n}{a_{\mathcal{A}}^0}j\,sin(k\,\Delta x)\\ -\alpha^n\,(\omega_{\mathcal{A}}^0)^2\,a_{\mathcal{A}}^0\,j\,sin(k\,\Delta x) & 1+2\,\alpha^n\,sin^2(k\,\Delta x/2)\end{bmatrix},\ \Delta=\det\mathbf{G}_{\mathcal{A}}.
\end{aligned}
\tag{38}
$$

G is a first eigenvalue related to the mass equation. As written in Appendix B, $|G|<1$ if $\mathscr{C}_{|u|}<\mathscr{C}_{|u|}^{\text{crit}}$. The two remaining eigenvalues are linked to the matrix $\mathbf{G}_{\mathcal{A}}^{-1}\,\mathbf{G}_{\mathcal{C}}$ which couples the momentum and the energy equations and can not be easily found analytically. Starting from $\mathscr{C}_{|u|}^{\text{crit}}$, a loop on all the k modes $\in[0,\,4\pi/\Delta x]$ is performed and the spectral radius $|G|_{\mathcal{AC}}^k$ associated to $\left(\mathbf{G}_{\mathcal{A}}^{-1}\,\mathbf{G}_{\mathcal{C}}\right)(k)$ is calculated. If, during the loop, $|G|_{\mathcal{AC}}^k>1$, then $\mathscr{C}_{|u|}^{\text{crit}}$ is slightly decreased and the loop is restarted.

Otherwise the current Courant number is stored and considered as the stable Courant number of the above von Neumann analysis.

On Figure 6 and Figure 7, the curve labeled "VN-Sp" (red line) displays the different stable convective Courant numbers obtained thanks to this method. A very good agreement holds with the empirical measures for all M_{min} above M_{thres}. Then, contrary to the numerical measures, the von Neumann method seems to reach the theoretical plateau $\lim_{M_{min}\to 0} \mathscr{C}^{th}_{|u|}(M_{min})$, at least for $M_{min} \in \left[7.5\times 10^{-2},\, 0.35\right]$. Unfortunately, for very low Mach numbers $\mathscr{C}_{|u|}$ plunges down. It predicts $\mathscr{C}_{|u|} = 10^{-2}$ when $M_{min} = 10^{-4}$. This might stem from the fact that the dynamics of the zeroth-order terms at time step t^{n+1} have been supposed constant to allow the derivation of the acoustic gain matrix. Yet, as formally shown in [23] by performing a Mach expansion on the non-conservative variables of the acoustic subsystem: when the reference Mach number is close to zero, the zeroth-order momentum term is fed by the second-order pressure gradient. Thus, one could assume that if the amplitude of this second-order pressure gradient explodes because of an instability, the zeroth-order momentum term would rise too so that to partially damp the instability. Further investigations should be done in order to better understand this sudden drop. As of now, one can simply have a look on the shape of the modulus of the eigenvalues $\left|\lambda^1_{\mathcal{AC}}\right|$ and $\left|\lambda^2_{\mathcal{AC}}\right|$ of $\mathbf{G}_{\mathcal{A}}^{-1}\,\mathbf{G}_{\mathcal{C}}$ seen as functions of the k mode $\in [0,\, 4\pi/\Delta x]$. Figure 10 and Figure 11 in Appendix E display $(k\,\Delta x)/(4\,\pi) \to |\lambda^r_{\mathcal{AC}}|\,,\ \forall r \in \{1,\, 2\}$ for $M_{min} = 10^{-3}$ and $\mathscr{C}_{|u|} = \mathscr{C}^{\text{crit}}_{|u|}$. It seems that the maximal value for $\left|\lambda^2_{\mathcal{AC}}\right|$ is reached in the neighborhood of $k \approx T_{\Delta x}/2$ with $T_{\Delta x} = 4\,\pi/\Delta x$. Then one can linearize $\mathbf{G}_{\mathcal{A}}^{-1}\,\mathbf{G}_{\mathcal{C}}(T_{\Delta x}/2 + \epsilon)$ and derive the analytical shape of the eigenvalues modulus up to a $O(\epsilon^2)$ term. After tedious calculations (see Appendix E), one can observe that the imaginary parts of the eigenvalues contain a $\mathscr{C}_{|u|}/M_{min}$ term which becomes preponderant as the Mach number tends towards zero.

7 Conclusion

The present work focuses on the derivation of an IMEX version of a Mach-sensitive fractional step introduced in [23]. The time-implicit scheme derived for the acoustic subsystem is based on the non-conservative dynamics of strong Riemann invariants provided by the relaxation schemes framework. Although such a technique stems from the Lagrange-Projection theory [11, 18], it can be extended to the present splitting because of density time invariance in the acoustic sub-step and the piece-wise constant structure of the computed solution. The resulting IMEX scheme is simple, the implicit part being inverted by hand, and conservative by construction. What is more, the maximum principle preservation for purely convected quantities holds under a non-restrictive condition for the time-explicit *convective flux*.

A low Mach number shock tube has highlighted a trade-off in the use of IMEX schemes. Indeed, if one is interested by pressure jumps through shock waves, then using an IMEX scheme with $\mathscr{C}_E \gg 1$ might be inappropriate if the accuracy of the shock profile is at stake. Besides, the gain in CPU time is not sufficient to compensate the implicit diffusion and dispersion errors: for the pressure variable, IMEX schemes are still less efficient than full time-explicit ones. However, any quantities varying only through material waves should be depicted more efficiently and with a sufficient accuracy.

Finally, stability measures performed in the case of an isolated contact discontinuity for different

Mach numbers seem to suggest that the present IMEX approach is uniformly stable for a convective Courant number $\mathscr{C}_{|u|}$ of the order of 0.3. A von Neumann-like stability analysis performed in the constant flow region where the instability spreads is in good agreement with the numerical observations for Mach numbers lying between 0.3 and 1. Further investigations should be undertaken to understand the sudden drop of the stable convective Courant number obtained with the von Neumann approach as the Mach number tends towards zero. As for the Lagrange-Projection approach, the Mach-uniform stability predicted in [36] has been found for $\mathscr{C}_{|u|} = 1$.

As pointed out along the introduction, the ultimate goal here is to derive an IMEX scheme able to accurately follow slow material waves *and*, when a strong shock wave occurs, even in the case of a low Mach number flow, to switch for a fully time-explicit Riemann solver. That is why, future works could deal with the design of an additional *global shock detector* criterion to complete the definition of the splitting parameter $\mathscr{E}_0^n$. Then, the resulting Mach-Shock-sensitive IMEX scheme might be better suited for a condensation induced water hammer scenario. What is more, at a given instant, the computational domain can feature subsonic areas as well as sonic or supersonic ones. Thus, the spatial dependence of the splitting parameter could also been examined. Indeed, provided that the consistency of the overall fractional step is not deteriorated, such a spatial dependence would allow to capture local fluctuations of the Mach number, and the present approach to react more finely.

Appendix A: Discrete Preservation of the Contact Discontinuity Riemann Invariants

Before focusing on the preservation of the contact discontinuity Riemann invariants property, let us have a look on the discrete momentum equation related to the flux (19).

$$
\begin{aligned}
&\text{Assume that: } u_i^{n+} = \frac{R_i^{n+} + W_i^{n+}}{2} \text{ ,then:} \\
&u_i^{n+1} = \frac{R_i^{n+1} + W_i^{n+1}}{2} \\
&\Leftrightarrow \frac{u_i^{n+1} - u_i^{n+}}{\Delta t} = \frac{1}{2}\left[\frac{R_i^{n+1} - R_i^{n+}}{\Delta t} + \frac{W_i^{n+1} - W_i^{n+}}{\Delta t}\right] \\
&\Leftrightarrow \frac{u_i^{n+1} - u_i^{n+}}{\Delta t} = -\frac{(1-(\mathscr{E}_0^n)^2)(a_{\mathcal{A}})^{n+}\,\tau_i^{n+}}{2}\left[\frac{R_i^{n+1} - R_{i-1}^{n+1}}{\Delta x} - \frac{W_{i+1}^{n+1} - W_i^{n+1}}{\Delta x}\right] \\
&\overset{\rho_i^{n+1}=\rho_i^{n+}}{\underset{\Leftrightarrow}{\frown}} \frac{\rho_i^{n+1}\,u_i^{n+1} - \rho_i^{n+}\,u_i^{n+}}{\Delta t} + \frac{(1-(\mathscr{E}_0^n)^2)\,(a_{\mathcal{A}})^{n+}}{\Delta x}\left[\frac{R_i^{n+1} - W_{i+1}^{n+1}}{2} - \frac{R_{i-1}^{n+1} - W_i^{n+1}}{2}\right] = 0 \\
&\Leftrightarrow \frac{\rho_i^{n+1}\,u_i^{n+1} - \rho_i^{n+}\,u_i^{n+}}{\Delta t} + (1-(\mathscr{E}_0^n)^2)\frac{(p_{\mathcal{A}}^*)_{i+1/2}^{n+1} - (p_{\mathcal{A}}^*)_{i-1/2}^{n+1}}{\Delta x} = 0, \\
&\text{with: } (p_{\mathcal{A}}^*)_{i+1/2}^{n+1} = (a_{\mathcal{A}})^{n+}\,\frac{R_i^{n+1} - W_{i+1}^{n+1}}{2}.
\end{aligned}
\tag{39}
$$

Thus:

$$
\begin{aligned}
&u_i^{n+} = \frac{R_i^{n+} + W_i^{n+}}{2}, \text{ and } u_i^{n+1} = \frac{R_i^{n+1} + W_i^{n+1}}{2} \Leftrightarrow \\
&u_i^{n+} = \frac{R_i^{n+} + W_i^{n+}}{2}, \text{ and } \frac{(\rho\,u)_i^{n+1} - (\rho\,u)_i^{n+}}{\Delta t} + (1-(\mathscr{E}_0^n)^2))\frac{(p_{\mathcal{A}}^*)_{i+1/2}^{n+1} - (p_{\mathcal{A}}^*)_{i-1/2}^{n+1}}{\Delta x} = 0.
\end{aligned}
\tag{40}
$$

Then, if $u_i^{n+} = \left(R_i^{n+} + W_i^{n+}\right)/2$, solving the momentum equation is strictly equivalent to directly setting $u_i^{n+1} = \left(R_i^{n+1} + W_i^{n+1}\right)/2$.

Discrete Preservation of the Riemann Invariants of a Contact Discontinuity

Consider an equation of state such that:

$$
(\rho\,\varepsilon)^{\text{EOS}}(\rho,\, p) = C(p)\,\rho + B(p), \tag{41}
$$

with $p \to C(p)$ and $p \to B(p)$ smooth functions such as $(\rho\,\varepsilon)_{|\rho}^{\text{EOS}} : p \to C(p)\,\rho + B(p)$ is injective on the domain of definition of p. Formula (41) belongs to the "T1-class" of EOS introduced in [16]. One can notice that the stiffened gas thermodynamics is included in this category. In the sequel, the exact invariance of velocity and pressure in the case of an isolated contact wave described in subsection 5.1.2 is checked.

Acoustic Sub-step

Assume that at the end of the convective sub-step, the isolated contact discontinuity has been preserved:

$$\begin{aligned} &\forall\, i:\ u_i^{n+} = u^0,\ p_i^{n+} = p^0, \\ \Rightarrow &\forall\, i:\ W_i^{n+} = u^0 - \frac{p^0}{a_{\mathcal{A}}^{n+}} = W^{0,\,n+},\ R_i^{n+} = u^0 + \frac{p^0}{a_{\mathcal{A}}^{n+}} = R^{0,\,n+}. \end{aligned} \tag{42}$$

Considering the discrete dynamics of W and R written in (17) coupled with the transparent boundary conditions $W_{N_{cells}+1}^{n+} = W_{N_{cells}}^{n+}$ and $W_0^{n+} = W_1^{n+}$, one can easily see that:

$$\forall\, i:\ W_i^{n+1} = W^{0,\,n+},\ R_i^{n+1} = R^{0,\,n+}. \tag{43}$$

Please note that the constant relaxation hypothesis $(a_{\mathcal{A}})^n = K \underset{i\in[1,\,N_{cells}]}{max} \left(\rho_i^n\,(c_{\mathcal{A}})_i^n\right),\ K > 1$, plays an important role here since a local value of $a_{\mathcal{A}}$ would have been sensible to the density discontinuity preventing W and R to remain constant. Thus, property (43) cannot be guaranteed in this case. Then, $(p_{\mathcal{A}}^*)_{i+1/2}^{n+1} = (p_{\mathcal{A}}^*)_{i-1/2}^{n+1} = a_{\mathcal{A}}^{n+}\left(R^{0,\,n+} - W^{0,\,n+}\right)/2$ and $(u_{\mathcal{A}}^*)_{i+1/2}^{n+1} = (u_{\mathcal{A}}^*)_{i-1/2}^{n+1} = \left(R^{0,\,n+} + W^{0,\,n+}\right)/2$ such that the discrete fluctuation of the time-implicit acoustic flux is null. The mass, momentum and the energy equations thus become:

$$\begin{aligned} &\frac{\rho_i^{n+1} - \rho_i^{n+}}{\Delta t} = 0, \\ &\rho_i^{n+}\frac{u_i^{n+1} - u_i^{n+}}{\Delta t} = 0, \\ &\rho_i^{n+}\frac{\left(\varepsilon_i^{n+1} - \varepsilon_i^{n+}\right) + \left((u_i^{n+1})^2/2 - (u_i^{n+})^2/2\right)}{\Delta t} = 0. \end{aligned} \qquad \begin{aligned} &\rho_i^{n+1} = \rho_i^{n+}, \\ \Rightarrow\ &u_i^{n+1} = u_i^{n+} = u^0, \\ &(\rho\,\varepsilon)^{\mathrm{EOS}}\left(\rho_i^{n+},\, p_i^{n+1}\right) = (\rho\,\varepsilon)^{\mathrm{EOS}}\left(\rho_i^{n+},\, p_i^{n+}\right). \end{aligned} \tag{44}$$

Since $(\rho\,\varepsilon)_{|\rho}^{\mathrm{EOS}} : p \to C(p)\,\rho + B(p)$ is injective, $p_i^{n+1} = p_i^{n+} = p^0$ and the acoustic sub-step exactly preserves the velocity and pressure uniform profiles.

Convective Sub-step

The convective flux associated to subsystem $\mathcal{C}$ is obtained using the same kind of relaxation method. Details are given in [23]. The convective flux formula at face $i+1/2$ reads:

$$\mathbf{H}_{\mathbf{c}}{}_{i+1/2}^{n} = \begin{cases} (\mathbf{F}_{\mathcal{C}})_i^n & \text{if } u_i^n - \mathscr{E}_0^n\,(a_{\mathcal{C}}^n)_{i+1/2}\tau_i^n > 0 \\ (\mathbf{F}_{\mathcal{C}})_{i+1/2}^{*,\,n} & \text{if } u_i^n - \mathscr{E}_0^n\,(a_{\mathcal{C}}^n)_{i+1/2}\tau_i^n \le 0 < (u_{\mathcal{C}}^*)_{i+1/2}^n \\ (\mathbf{F}_{\mathcal{C}})_{i+1/2}^{**,\,n} & \text{if } (u_{\mathcal{C}}^*)_{i+1/2}^n \le 0 < u_{i+1}^n + \mathscr{E}_0^n\,(a_{\mathcal{C}}^n)_{i+1/2}\tau_{i+1}^n \\ (\mathbf{F}_{\mathcal{C}})_{i+1}^n & \text{if } u_{i+1}^n + \mathscr{E}_0^n\,(a_{\mathcal{C}}^n)_{i+1/2}\tau_{i+1}^n \le 0 \\ (a_{\mathcal{C}}^n)_{i+1/2} = & K\,max\left(\rho_i^n\,(c_{\mathcal{C}})_i^n,\, \rho_{i+1}^n\,(c_{\mathcal{C}})_{i+1}^n\right),\ K > 1 \\ \mathbf{F}_{\mathcal{C}}\,(\mathbf{U}) = & \left[\rho\,u,\, \rho\,u^2 + \mathscr{E}_0^2\,p,\, (\rho\,e + \mathscr{E}_0^2\,p)\,u\right]^T, \end{cases} \tag{45}$$

with :

$$
\begin{aligned}
(\mathbf{F}_{\mathcal{C}})^{*,n}_{i+1/2} &= \begin{bmatrix} (\rho^*_{\mathcal{C}})^n_i \, (u^*_{\mathcal{C}})^n_{i+1/2} \\ (\rho^*_{\mathcal{C}})^n_i \left((u^*_{\mathcal{C}})^n_{i+1/2}\right)^2 + (\mathscr{E}_0^n)^2 (\Pi^*_{\mathcal{C}})^n_{i+1/2} \\ \left((\rho^*_{\mathcal{C}}\, e^*_{\mathcal{C}})^n_i + (\mathscr{E}_0^n)^2 (\Pi^*_{\mathcal{C}})^n_{i+1/2}\right) (u^*_{\mathcal{C}})^n_{i+1/2} \end{bmatrix}, \\
(\mathbf{F}_{\mathcal{C}})^{**,n}_{i+1/2} &= \begin{bmatrix} (\rho^*_{\mathcal{C}})^n_{i+1} \, (u^*_{\mathcal{C}})^n_{i+1/2} \\ (\rho^*_{\mathcal{C}})^n_{i+1} \left((u^*_{\mathcal{C}})^n_{i+1/2}\right)^2 + (\mathscr{E}_0^n)^2 (\Pi^*_{\mathcal{C}})^n_{i+1/2} \\ \left((\rho^*_{\mathcal{C}}\, e^*_{\mathcal{C}})^n_{i+1} + (\mathscr{E}_0^n)^2 (\Pi^*_{\mathcal{C}})^n_{i+1/2}\right) (u^*_{\mathcal{C}})^n_{i+1/2} \end{bmatrix}, \\
(u^*_{\mathcal{C}})^n_{i+1/2} &= \frac{u^n_{i+1} + u^n_i}{2} - \frac{\mathscr{E}_0^n}{2\,(a_{\mathcal{C}})^n_{i+1/2}} \left(p^n_{i+1} - p^n_i\right), \\
(\mathscr{E}_0^n)^2 \, (\Pi^*_{\mathcal{C}})^n_{i+1/2} &= (\mathscr{E}_0^n)^2 \, \frac{p^n_{i+1} + p^n_i}{2} - \frac{\mathscr{E}_0^n \, (a_{\mathcal{C}})^n_{i+1/2}}{2} \left(u^n_{i+1} - u^n_i\right), \\
(\rho^*_{\mathcal{C}})^n_k &= 1/(\tau^*_{k,\mathcal{C}})^n, \;\; (\tau^*_{k,\mathcal{C}})^n = \tau^n_k + \frac{(-1)^{J_k+1}}{\mathscr{E}_0^n \, (a_{\mathcal{C}})^n_{i+1/2}} \left((u^*_{\mathcal{C}})^n_{i+1/2} - u^n_k\right), \\
(e^*_{\mathcal{C}})^n_k &= e^n_k + \mathscr{E}_0^n \, \frac{(-1)^{J_k}}{(a_{\mathcal{C}})^n_{i+1/2}} \left((\Pi^*_{\mathcal{C}}\, u^*_{\mathcal{C}})^n_{i+1/2} - p^n_k \, u^n_k\right), \\
k &\in \{i,\, i+1\}, \;\; J_i = 1, \;\; J_{i+1} = 2.
\end{aligned}
\tag{46}
$$

In the case of an isolated contact discontinuity with $\underline{u^0 > 0}$, the convective flux writes:

$$
\mathbf{H}_{\mathbf{c}}{}^{n,\,\mathrm{Contact}}_{i+1/2} = \begin{bmatrix} \rho^n_i \, u^0 \\ \rho^n_i \, (u^0)^2 + (\mathscr{E}_0^n)^2 \, p^0 \\ (\rho\,\varepsilon)^{\mathrm{EOS}} \left(\rho^n_i,\, p^0\right) \, u^0 + \rho^n_i \, \dfrac{(u^0)^3}{2} + (\mathscr{E}_0^n)^2 \, p^0 \, u^0 \end{bmatrix}. \tag{47}
$$

The mass, momentum and energy dynamics then read:

$$
\begin{aligned}
&\frac{\rho^{n+}_i - \rho^n_i}{\Delta t} + u^0 \frac{\rho^n_i - \rho^n_{i-1}}{\Delta x} = 0, \\
&\frac{\rho^{n+}_i u^{n+}_i - \rho^n_i u^0}{\Delta t} + (u^0)^2 \frac{\rho^n_i - \rho^n_{i-1}}{\Delta x} = 0, \\
&\frac{(\rho\,\varepsilon)^{\mathrm{EOS}} \left(\rho^{n+}_i,\, p^{n+}_i\right) - (\rho\,\varepsilon)^{\mathrm{EOS}} \left(\rho^n_i,\, p^0\right)}{\Delta t} + \frac{1}{2} \frac{\rho^{n+}_i (u^{n+}_i)^2 - \rho^n_i (u^0)^2}{\Delta t} \\
&+ u^0 \frac{(\rho\,\varepsilon)^{\mathrm{EOS}} \left(\rho^n_i,\, p^0\right) - (\rho\,\varepsilon)^{\mathrm{EOS}} \left(\rho^n_{i-1},\, p^0\right)}{\Delta x} + \frac{(u^0)^3}{2} \frac{\rho^n_i - \rho^n_{i-1}}{\Delta x} = 0.
\end{aligned}
\tag{48}
$$

By rewriting $\rho^{n+}_i u^{n+}_i - \rho^n_i u^0$ as $\rho^{n+}_i \left(u^{n+}_i - u^0\right) + \left(\rho^{n+}_i - \rho^n_i\right) u^0$ and using the discrete mass equation, the momentum equation can be simplified:

$$
\rho^{n+}_i \frac{u^{n+}_i - u^0}{\Delta t} = 0 \Rightarrow u^{n+}_i = u^0. \tag{49}
$$

The kinetic part in the discrete energy equation then vanishes by factorizing by $(u^0)^2/2$ and using, once again, the discrete mass equation. Injecting formula (41), one obtains:

$$\frac{C(p_i^{n+})\rho_i^{n+} + B(p_i^{n+}) - \left(C(p^0)\rho_i^n + B(p^0)\right)}{\Delta t} + u^0 \frac{C(p^0)\left(\rho_i^n - \rho_{i-1}^n\right)}{\Delta x} = 0. \tag{50}$$

The linear behavior of $(\rho\,\varepsilon)^{\mathrm{EOS}}_{|p} : \rho \to C(p)\,\rho + B(p)$ as well as the fact that $C(p) = C(p^0)$ is a constant in this configuration, play an important role. Indeed, it allows to retrieve the discrete mass equation by factorizing by $C(p^0)$. Finally, one obtains:

$$\begin{aligned} &\frac{C(p_i^{n+})\rho_i^{n+} + B(p_i^{n+}) - \left(C(p^0)\rho_i^{n+} + B(p^0)\right)}{\Delta t} = 0 \\ \Leftrightarrow &\frac{(\rho\,\varepsilon)^{\mathrm{EOS}}\left(\rho_i^{n+},\, p_i^{n+}\right) - (\rho\,\varepsilon)^{\mathrm{EOS}}\left(\rho_i^{n+},\, p^0\right)}{\Delta t} = 0. \end{aligned} \tag{51}$$

Using the fact that $(\rho\,\varepsilon)^{\mathrm{EOS}}_{|\rho_i^{n+}} : p \to C(p)\,\rho_i^{n+} + B(p)$ is injective, it results in $p_i^{n+} = p^0$.

Appendix B: Study of the von Neumann Gain Matrices

This appendix is dedicated to the study of the von Neumann gain matrices written in (33) and (38). The derivation of the convective gain matrix being relatively straightforward, special attention is paid to the expression of its eigenvalues as well as a sufficient condition ensuring that their modulus is strictly lower than one. Besides, the derivation of the acoustic gain matrix is completely done.

Analysis of the Convective Gain Matrix Eigenvalues

Let us consider the von Neumann gain matrix associated with the convective sub-step:

$$\begin{bmatrix} G & -\dfrac{\rho^0\,\mathscr{C}_{|u|}}{|u^0|}\,j\,sin(k\,\Delta x) & 0 \\ 0 & G & -\dfrac{(\mathscr{E}_0^n)^2\,\mathscr{C}_{|u|}}{\rho^0\;|u^0|}\,j\,sin(k\,\Delta x) \\ 0 & -\dfrac{\rho^0\,(c_{\mathcal{C}}^0)^2\,\mathscr{C}_{|u|}}{|u^0|}\,j\,sin(k\,\Delta x) & G \end{bmatrix}, \tag{52}$$

$$\text{and: } G = 1 - 2\frac{\mathscr{C}_{|u|}}{\mathscr{C}_{|u|}^{\mathrm{crit}}}\,sin^2(k\,\Delta x/2) - j\,\frac{u^0}{|u^0|}\mathscr{C}_{|u|}\,sin(k\,\Delta x),$$

$$\text{with: } \mathscr{C}_{|u|}^{\mathrm{crit}} = \left|u^0\right| / \left|\lambda^0\right| \in]0,\,1[\,.$$

G is the first eigenvalue of this matrix. Define $X = sin^2(k\,\Delta x/2) \in [0,\,1]$, then $sin^2(k\,\Delta x) = 4\,X\,(1-X)$. Thus:

$$
\begin{aligned}
|G|^2 &= \left(1 - 2\frac{\mathscr{C}_{|u|}}{\mathscr{C}_{|u|}^{\text{crit}}}\,X\right)^2 + 4\,\mathscr{C}_{|u|}^2\,X\,(1-X),\\
|G|^2 < 1 &\Leftrightarrow \mathscr{C}_{|u|} < \frac{\mathscr{C}_{|u|}^{\text{crit}}}{\left((1-(\mathscr{C}_{|u|}^{\text{crit}})^2)\,X + (\mathscr{C}_{|u|}^{\text{crit}})^2\right)}.
\end{aligned}
\tag{53}
$$

Since $X \in [0,1]$ the most constraining CFL condition is $\mathscr{C}_{|u|} < \mathscr{C}_{|u|}^{\text{crit}}$.

The two other eigenvalues of the above gain matrix are the roots of the characteristic polynomial function:

$$
(G-\lambda)^2 + (\mathscr{E}_0^n)^2\,(\mathscr{C}_{|u|})^2\left(\frac{c_{\mathcal{C}}^0}{u^0}\right)^2 sin^2(k\,\Delta x). \tag{54}
$$

They write:

$$
\begin{aligned}
\lambda^{\pm} &= G \mp j\,\mathscr{E}_0^n\,\mathscr{C}_{|u|}\left|\frac{c_{\mathcal{C}}^0}{u^0}\right|\,|sin(k\,\Delta x)|\,,\\
|\lambda^{\pm}|^2 &= \left(1 - 2\frac{\mathscr{C}_{|u|}}{\mathscr{C}_{|u|}^{\text{crit}}}\,X\right)^2 + \mathscr{C}_{|u|}^2\left([1 + (\mathscr{E}_0^n)^2\left|\frac{c_{\mathcal{C}}^0}{u^0}\right|^2]\,4\,X\,(1-X) \pm 2\mathscr{E}_0^n\frac{u^0}{|u^0|}\left|\frac{c_{\mathcal{C}}^0}{u^0}\right| sin(k\,\Delta x)\;|sin(k\,\Delta x)|\right)\\
\Rightarrow |\lambda^{\pm}|^2 &\le \left(1 - 2\frac{\mathscr{C}_{|u|}}{\mathscr{C}_{|u|}^{\text{crit}}}\,X\right)^2 + 4\left(1 + \mathscr{E}_0^n\left|\frac{c_{\mathcal{C}}^0}{u^0}\right|\right)^2\mathscr{C}_{|u|}^2\,X\,(1-X) = \left(1 - 2\frac{\mathscr{C}_{|u|}}{\mathscr{C}_{|u|}^{\text{crit}}}\,X\right)^2 + 4\left(\frac{\mathscr{C}_{|u|}}{\mathscr{C}_{|u|}^{\text{crit}}}\right)^2 X\,(1-X).
\end{aligned}
\tag{55}
$$

A sufficient condition ensuring that $|\lambda^{\pm}| < 1$ is once again $\mathscr{C}_{|u|} < \mathscr{C}_{|u|}^{\text{crit}}$.

Derivation of the Linearized Acoustic Dynamics

The von Neumann analysis has to be made on the relaxation system (9). Define at time t^{n+}:

$$
\begin{aligned}
W_i^{n+} &= u_i^{n+} - \frac{p_i^{n+}}{a_{\mathcal{A}}^{n+}} = u_i^{n+} - \frac{\Pi_i^{n+}}{a_{\mathcal{A}}^{n+}},\\
R_i^{n+} &= u_i^{n+} + \frac{p_i^{n+}}{a_{\mathcal{A}}^{n+}} = u_i^{n+} + \frac{\Pi_i^{n+}}{a_{\mathcal{A}}^{n+}}.
\end{aligned}
\tag{56}
$$

Then,

$$
\left\{
\begin{array}{l}
\dfrac{\rho_i^{n+1}-\rho_i^{n+}}{\Delta t}=0,\\
\dfrac{(\rho\,u)_i^{n+1}-(\rho\,u)_i^{n+}}{\Delta t}+\left(1-(\mathscr{E}_0^n)^2\right)\dfrac{(p_{\mathcal{A}}^*)_{i+1/2}^{n+1}-(p_{\mathcal{A}}^*)_{i-1/2}^{n+1}}{\Delta x}=0,\\
\dfrac{(\rho\,\Pi)_i^{n+1}-(\rho\,\Pi)_i^{n+}}{\Delta t}+\left(1-(\mathscr{E}_0^n)^2\right)(a_{\mathcal{A}}^{n+})^2\dfrac{(u_{\mathcal{A}}^*)_{i+1/2}^{n+1}-(u_{\mathcal{A}}^*)_{i-1/2}^{n+1}}{\Delta x}=0,\\
\dfrac{(\rho\,e)_i^{n+1}-(\rho\,e)_i^{n+}}{\Delta t}+\left(1-(\mathscr{E}_0^n)^2\right)\dfrac{(p_{\mathcal{A}}^*\,u_{\mathcal{A}}^*)_{i+1/2}^{n+1}-(p_{\mathcal{A}}^*\,u_{\mathcal{A}}^*)_{i-1/2}^{n+1}}{\Delta x}=0,
\end{array}
\right.
$$

$$\Leftrightarrow$$

$$
\left\{
\begin{array}{ll}
\dfrac{\rho_i^{n+1}-\rho_i^{n+}}{\Delta t} & =0,\\
\dfrac{(\rho\,u)_i^{n+1}-(\rho\,u)_i^{n+}}{\Delta t} & +\left(1-(\mathscr{E}_0^n)^2\right)\left[\dfrac{\Pi_{i+1}^{n+1}-\Pi_{i-1}^{n+1}}{2\,\Delta x}-\dfrac{a_{\mathcal{A}}^{n+}}{2}\dfrac{u_{i+1}^{n+1}-2\,u_i^{n+1}+u_{i-1}^{n+1}}{\Delta x}\right]=0,\\
\dfrac{(\rho\,\Pi)_i^{n+1}-(\rho\,\Pi)_i^{n+}}{\Delta t} & +\left(1-(\mathscr{E}_0^n)^2\right)\left[(a_{\mathcal{A}}^{n+})^2\dfrac{u_{i+1}^{n+1}-u_{i-1}^{n+1}}{2\,\Delta x}-\dfrac{a_{\mathcal{A}}^{n+}}{2}\dfrac{\Pi_{i+1}^{n+1}-2\,\Pi_i^{n+1}+\Pi_{i-1}^{n+1}}{\Delta x}\right]=0,\\
\dfrac{(\rho\,e)_i^{n+1}-(\rho\,e)_i^{n+}}{\Delta t} & +\left(1-(\mathscr{E}_0^n)^2\right)[\dfrac{(\Pi\,u)_{i+1}^{n+1}-(\Pi\,u)_{i-1}^{n+1}}{2\,\Delta x}-\dfrac{1}{4\,a_{\mathcal{A}}^{n+}}\dfrac{(\Pi^2)_{i+1}^{n+1}-2\,(\Pi^2)_i^{n+1}+(\Pi^2)_{i-1}^{n+1}}{\Delta x}\\
 & -\dfrac{a_{\mathcal{A}}^{n+}}{4}\dfrac{(u^2)_{i+1}^{n+1}-2\,(u^2)_i^{n+1}+(u^2)_{i-1}^{n+1}}{\Delta x}]=0.
\end{array}
\right.
\tag{57}
$$

Supposing that $\forall\phi\in\{\rho,\,u,\,\Pi,\,e\}\,,\ \phi_i^{0,n+1}=\phi^0$ a constant, one can extract the linearized dynamics related to (57):

$$
\begin{array}{l}
\dfrac{\rho_i^{1,\,n+1}-\rho_i^{1,\,n+}}{\Delta t}=0,\\
\rho^0\dfrac{u_i^{1,\,n+1}-u_i^{1,\,n+}}{\Delta t}+\left(1-(\mathscr{E}_0^n)^2\right)\left[\dfrac{\Pi_i^{1,\,n+1}-\Pi_i^{1,\,n+1}}{2\,\Delta x}-\dfrac{a_{\mathcal{A}}^0}{2}\dfrac{u_{i+1}^{1,\,n+1}-2\,u_i^{1,\,n+1}+u_{i-1}^{1,\,n+1}}{\Delta x}\right]=0,\\
\rho^0\dfrac{\Pi_i^{1,\,n+1}-\Pi_i^{1,\,n+}}{\Delta t}+\left(1-(\mathscr{E}_0^n)^2\right)\left[(a_{\mathcal{A}}^0)^2\dfrac{u_i^{1,\,n+1}-u_i^{1,\,n+1}}{2\,\Delta x}-\dfrac{a_{\mathcal{A}}^0}{2}\dfrac{\Pi_{i+1}^{1,\,n+1}-2\,\Pi_i^{1,\,n+1}+\Pi_{i-1}^{1,\,n+1}}{\Delta x}\right]=0,\\
\rho^0\dfrac{e_i^{1,\,n+1}-e_i^{1,\,n+}}{\Delta t}+\left(1-(\mathscr{E}_0^n)^2\right)\left[p^0\dfrac{u_i^{1,\,n+1}-u_i^{1,\,n+1}}{2\,\Delta x}+u^0\dfrac{\Pi_i^{1,\,n+1}-\Pi_i^{1,\,n+1}}{2\,\Delta x}\right]\\
\qquad\qquad-\left(1-(\mathscr{E}_0^n)^2\right)\left[\dfrac{p^0}{a_{\mathcal{A}}^0}\dfrac{\Pi_{i+1}^{1,\,n+1}-2\,\Pi_i^{1,\,n+1}+\Pi_{i-1}^{1,\,n+1}}{2\,\Delta x}+u^0\,a_{\mathcal{A}}^0\dfrac{u_{i+1}^{1,\,n+1}-2\,u_i^{1,\,n+1}+u_{i-1}^{1,\,n+1}}{2\,\Delta x}\right]=0.
\end{array}
\tag{58}
$$

During the projection step, $\Pi_i^{n+1}=p_i^{n+1}=p^{EOS}\left(\rho_i^{n+1},\,\varepsilon_i^{n+1}\right)$ is imposed with $\varepsilon_i^{n+1}=e_i^{n+1}-(u_i^{n+1})^2/2$. If one assumes that this projection holds separately for zeroth order and first order terms then $\forall\sharp\in\{n+,\,n+1\}$:

$$\Pi_i^{1,\sharp} = p_i^{1,\sharp} = (\partial_\rho p_{|\varepsilon})^0 \, \rho_i^{1,\sharp} + (\partial_\varepsilon p_{|\rho})^0 \, \left(e_i^{1,\sharp} - u^0 \, u_i^{1,\sharp} \right). \tag{59}$$

Using the momentum equation, the perturbed pressure dynamics is then:

$$\frac{p_i^{1,n+1} - p_i^{1,n+}}{\Delta t} + \left(1 - (\mathscr{E}_0^n)^2\right) \left(\partial_\varepsilon p_{|\rho})\right)^0 \frac{p^0}{\rho^0} \left[\frac{u_{i+1}^{1,n+1} - u_{i-1}^{1,n+1}}{2\,\Delta x} - \frac{1}{a_{\mathcal{A}}^0} \frac{p_{i+1}^{1,n+1} - 2\,p_i^{1,n+1} + p_{i-1}^{1,n+1}}{2\,\Delta x} \right] = 0. \tag{60}$$

According to definition (6), $\left(\partial_\varepsilon p_{|\rho})\right)^0 \frac{p^0}{\rho^0}$ is exactly equal to $\rho^0 \, (c_{\mathcal{A}}^0)^2$. The linearized dynamics of the non conservative variables related to the acoustic scheme is then:

$$\begin{aligned}
&\frac{\rho_i^{1,n+1} - \rho_i^{1,n+}}{\Delta t} = 0, \\
&\frac{u_i^{1,n+1} - u_i^{1,n+}}{\Delta t} + \left(1 - (\mathscr{E}_0^n)^2\right) \left[\frac{1}{\rho^0} \frac{p_{i+1}^{1,n+1} - p_{i-1}^{1,n+1}}{2\,\Delta x} - \frac{a_{\mathcal{A}}^0}{\rho^0} \frac{u_{i+1}^{1,n+1} - 2\,u_i^{1,n+1} + u_{i-1}^{1,n+1}}{2\,\Delta x} \right] = 0, \\
&\frac{p_i^{1,n+1} - p_i^{1,n+}}{\Delta t} + \left(1 - (\mathscr{E}_0^n)^2\right) \rho^0 \, (c_{\mathcal{A}}^0)^2 \left[\frac{u_{i+1}^{1,n+1} - u_{i-1}^{1,n+1}}{2\,\Delta x} - \frac{1}{a_{\mathcal{A}}^0} \frac{p_{i+1}^{1,n+1} - 2\,p_i^{1,n+1} + p_{i-1}^{1,n+1}}{2\,\Delta x} \right] = 0.
\end{aligned} \tag{61}$$

Appendix C: Location of the IMEX Instability

Figure 8 and Figure 9 show the growth of the numerical instability observed in the case presented in subsection 5.1.2. The picture is taken at time $t = 2.496 \times 10^{-2}\, s$ but for a mesh of 10^3 cells (Figure 8) and for a finer one of 5×10^3 cells (Figure 9).

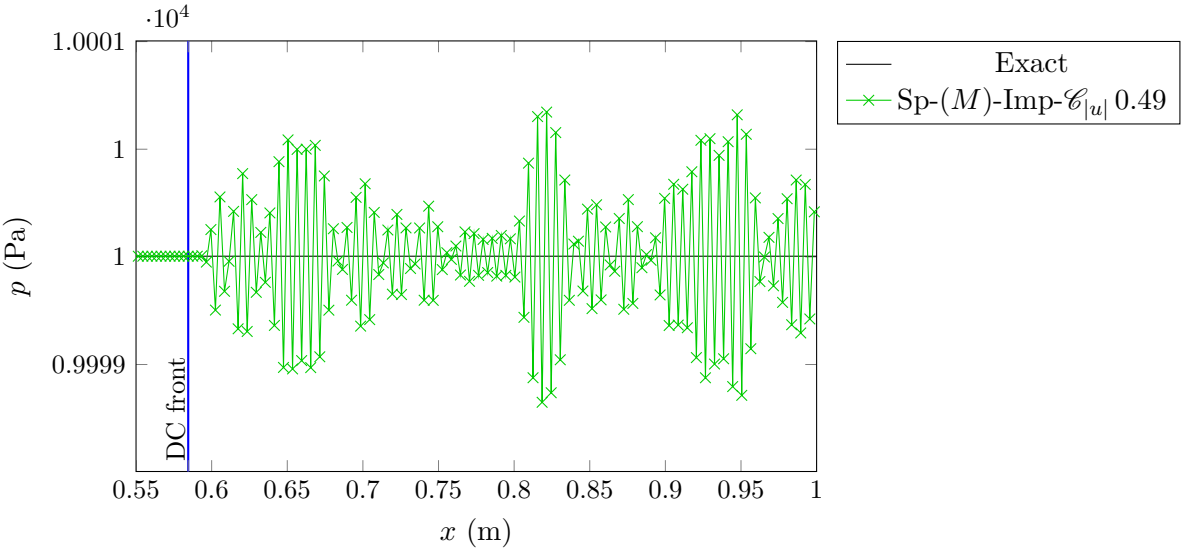

Figure 8: p, Perfect Gas, $M_{min} = 10^{-2}$, with $\mathbf{N_{cells}} = \mathbf{10^3}$, $\mathscr{C}_{|u|} = 0.49$, iteration 270, $(t = 2.496 \times 10^{-2}\ s)$

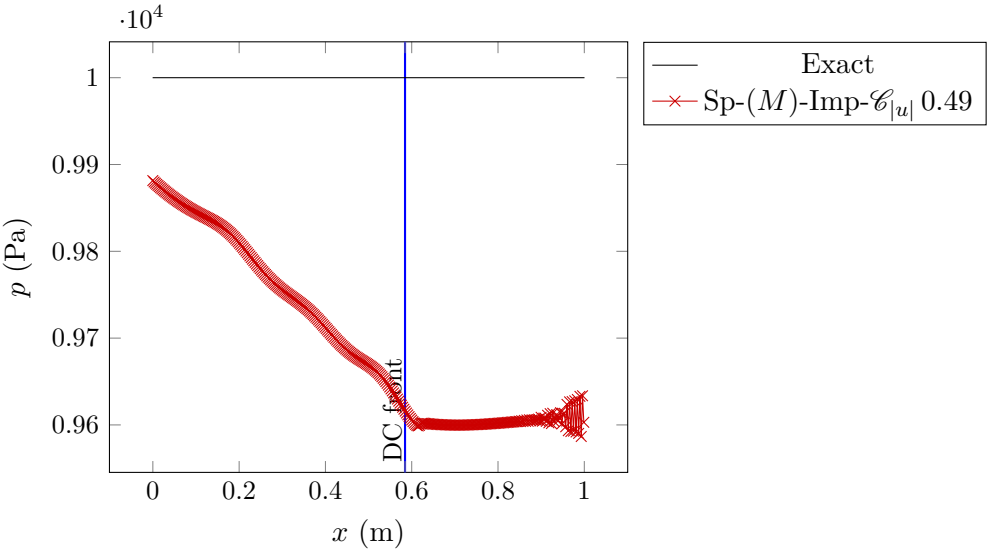

Figure 9: p, Perfect Gas, $M_{min} = 10^{-2}$, with $\mathbf{N_{cells}} = \mathbf{5 \times 10^3}$, $\mathscr{C}_{|u|} = 0.49$, iteration 1399, $(t = 2.497 \times 10^{-2}\ s)$

One can observe than the instability originates from the region located after the contact discontinuity front where the Mach number takes its lowest value. As the mesh is refined, the amplitude of the instability surges considerably since the numerical diffusion is largely diminished.

Appendix D: The Most Constraining Euler Courant Number

Let us consider the shock tube test case presented in subsection 5.2. The fastest Euler eigenvalue is $u^* + c_R^{0,*}$ with $c_R^{0,*} = c\left(\rho_R^*,\, p^*\right)$. It corresponds to the characteristic colliding with the 3-shock wave front speed. Here u^* and p^* are the intermediate velocity and pressure whose values can be approximatively calculated: $u^* \approx 1.49886\ m\,s^{-1}$, $p^* \approx 10020.9\ Pa$. What is more, the conservation of entropy through the 3-shock brings: $\rho_R^* = \rho_R^0 \left(p^*/p_R^0\right)^{1/\gamma}$, and $c\left(\rho_R^*,\, p^*\right) = c_R^0 \left(p^*/p_R^0\right)^{(\gamma-1)/\gamma} \approx 336.36256\ m\,s^{-1}$.

The most constraining time step got from the above wave speed writes:

$$\Delta t_E^{0,*} = \frac{\mathscr{C}_E^{0,*}}{2} \frac{\Delta x}{u^* + c_R^{0,*}}. \tag{62}$$

Besides the time step related to u^0 writes simply $\Delta t_{\mathcal{C}}^{u^0} = \mathscr{C}_{|u|}^{u^0}\, \Delta x / u^0$. Then:

$$\Delta t_{\mathcal{C}}^{u^0} = \Delta t_E^{0,*} \Leftrightarrow \mathscr{C}_{|u|}^{u^0} = \frac{u^0}{2\left(u^* + c_R^{0,*}\right)} \mathscr{C}_E^{0,*} \approx 1.48649 \times 10^{-3}\, \mathscr{C}_E^{0,*}. \tag{63}$$

Appendix E: Eigenvalues of a Linearized Unstable Gain Matrix of the Whole IMEX Scheme

Figure 10 and Figure 11 display the profile of the von Neumann gain matrices eigenvalues as function of the non-dimensional mode $\dfrac{k\,\Delta x}{4\,\pi}$. The Mach number is $M_{min} = 10^{-3}$ and the convective Courant number has deliberately been imposed equal to $\mathscr{C}_{|u|}^{\text{crit}}$, the critical Courant number ensuring the spectral radius of the convective gain matrix to be lower than one. The eigenvalues of $\mathbf{G}_{\mathcal{A}}^{-1}\,\mathbf{G}_{\mathcal{C}}$ are plotted in blue whereas those of $\mathbf{G}_{\mathcal{C}}$ (respectively $\mathbf{G}_{\mathcal{A}}^{-1}$) are plotted in red (respectively green). See (38) for the expressions of the gain matrices.

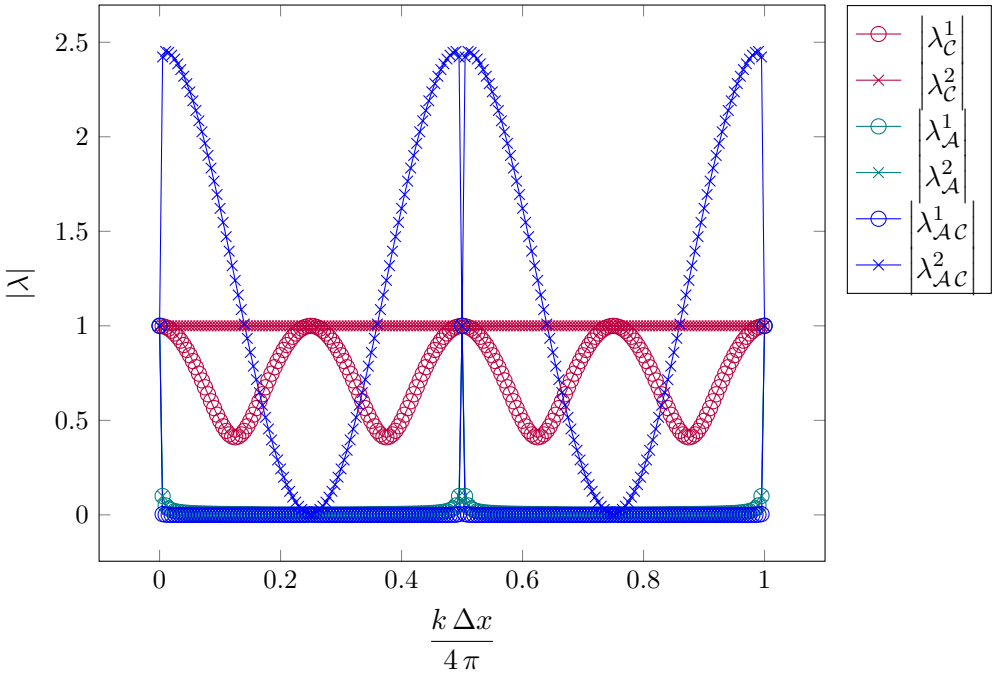

Figure 10: spectral radius of the different matrices, $M_{min} = 10^{-3}$, $\mathscr{C}_{|u|} = \mathscr{C}_{|u|}^{\text{crit}}$

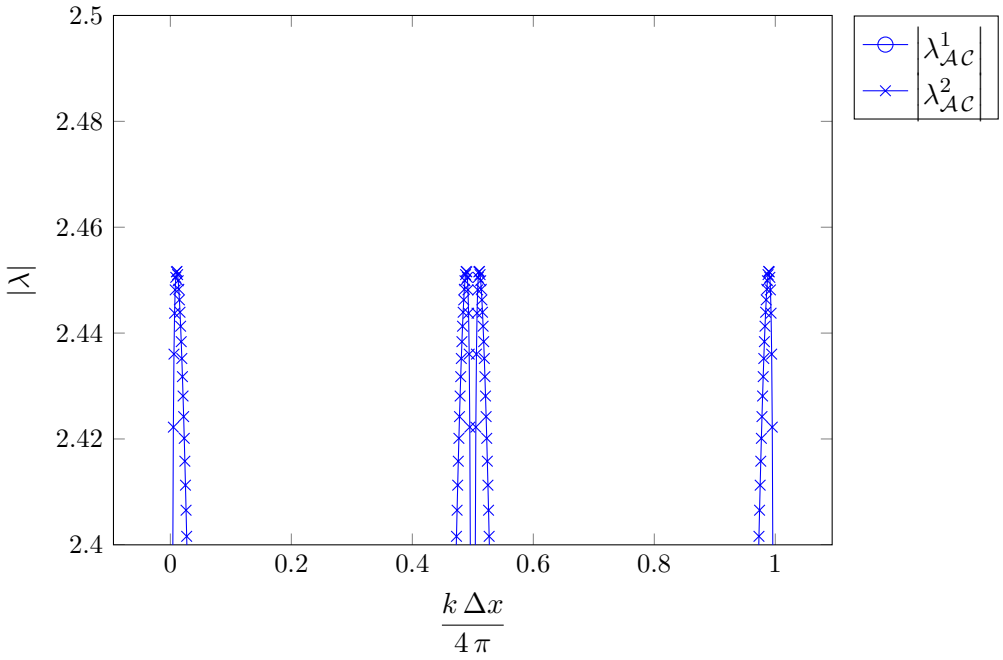

Figure 11: spectral radius of the different matrices, $M_{min} = 10^{-3}$, $\mathscr{C}_{|u|} = \mathscr{C}_{|u|}^{\text{crit}}$

According to Figure 10 and Figure 11 the maximal spectral radius of the von Neumann gain matrix is obtained in the neighborhood of $k = T_{\Delta x}/2$ with $T_{\Delta x} = 4\,\pi/\Delta x$. Assume than the wave number k is equal to $T_{\Delta x}/2 + \epsilon$, with ϵ a small perturbation. Then:

$$\begin{aligned} sin(k\,\Delta x/2) &= sin(\pi + (\epsilon\,\Delta x)/2) = -\frac{\epsilon\,\Delta x}{2} + O(\epsilon^3), \\ 2\,sin^2(k\,\Delta x/2) &= \frac{(\epsilon\,\Delta x)^2}{2} + O(\epsilon^4), \\ sin(k\,\Delta x) &= sin(2\,\pi + \epsilon\,\Delta x) = \epsilon\,\Delta x + O(\epsilon^3). \end{aligned} \tag{64}$$

In the sequel, one tries to compute the eigenvalues of the whole von Neumann gain matrix $\mathbf{G}_{\mathcal{A}}^{-1}\,\mathbf{G}_{\mathcal{C}}$ truncating order $O(\epsilon^3)$ terms. For the sake of simplicity $\epsilon\,\Delta x$ is now written ϵ.

Convective Gain Matrix:

The diagonal term of the convective gain matrix in equation (38) can be written:

$$G = 1 - 2\frac{\mathscr{C}_{|u|}}{\mathscr{C}_{|u|}^{\text{crit}}}\,sin^2(k\,\Delta x/2) - j\,\frac{u^0}{|u^0|}\mathscr{C}_{|u|}\,sin(k\,\Delta x) = 1 - \epsilon\,j\,\mathscr{C}_{|u|} - \frac{\mathscr{C}_{|u|}}{\mathscr{C}_{|u|}^{\text{crit}}}\frac{\epsilon^2}{2} + O(\epsilon^3). \tag{65}$$

The convective gain matrix then writes:

$$\mathbf{G}_{\mathcal{C}} = \begin{bmatrix} 1 - \epsilon\,j\,\mathscr{C}_{|u|} - \dfrac{\mathscr{C}_{|u|}}{\mathscr{C}_{|u|}^{\text{crit}}}\dfrac{\epsilon^2}{2} & -\epsilon\,j\dfrac{(\mathscr{E}_0^n)^2\,\mathscr{C}_{|u|}}{\rho^0\;|u^0|} \\ -\epsilon\,j\dfrac{\rho^0\,(c_{\mathcal{C}}^0)^2\,\mathscr{C}_{|u|}}{|u^0|} & 1 - \epsilon\,j\,\mathscr{C}_{|u|} - \dfrac{\mathscr{C}_{|u|}}{\mathscr{C}_{|u|}^{\text{crit}}}\dfrac{\epsilon^2}{2} \end{bmatrix} + O(\epsilon^3). \tag{66}$$

Acoustic Gain Matrix:

The acoustic gain matrix is:

$$\begin{aligned} &\mathbf{G}_{\mathcal{A}} = \begin{bmatrix} 1 + \dfrac{\epsilon^2}{2}\alpha^n & \epsilon\,j\dfrac{\alpha^n}{a_{\mathcal{A}}^0} \\ \epsilon\,j\,\alpha^n\,(\omega_{\mathcal{A}}^0)^2\,a_{\mathcal{A}}^0 & 1 + \dfrac{\epsilon^2}{2}\,\alpha^n\,(\omega_{\mathcal{A}}^0)^2 \end{bmatrix} + O(\epsilon^3), \\ &\text{with: } \alpha^n = \left(1 - (\mathscr{E}_0^n)^2\right)\frac{a_{\mathcal{A}}^0\,\mathscr{C}_{|u|}}{\rho^0\;|u^0|},\; a_{\mathcal{A}}^0 = \rho^0\,c^0, \\ &\text{and: } \omega_{\mathcal{A}}^0 = \frac{\rho^0\,c_{\mathcal{A}}^0}{a_{\mathcal{A}}^0} = \frac{c_{\mathcal{A}}^0}{c^0}. \end{aligned} \tag{67}$$

The determinant of such matrix writes easily:

$$\Delta = \det\mathbf{G}_{\mathcal{A}} = 1 + \frac{\epsilon^2\,\alpha^n}{2}\left(1 + (\omega_{\mathcal{A}}^0)^2\,(1 + 2\,\alpha^n)\right) + O(\epsilon^4), \tag{68}$$

and:

$$\mathbf{G}_{\mathcal{A}}^{-1} = \frac{1}{\Delta}\begin{bmatrix} 1+\dfrac{\epsilon^2}{2}\,\alpha^n\,(\omega_{\mathcal{A}}^0)^2 & -\epsilon\,j\dfrac{\alpha^n}{a_{\mathcal{A}}^0} \\ -\epsilon\,j\,\alpha^n\,(\omega_{\mathcal{A}}^0)^2\,a_{\mathcal{A}}^0 & 1+\dfrac{\epsilon^2}{2}\alpha^n \end{bmatrix} + O(\epsilon^3). \tag{69}$$

Please note that, by construction, the term α^n is of the order of $1/M^0$ with $M^0 = \left|u^0\right|/c^0$ whereas $\omega_{\mathcal{A}}^0$ is an order one term with respect to M^0.

Acoustic-Convective Gain Matrix:

Neglecting punctually $1/\Delta$, each term of the product $\mathbf{G}_{\mathcal{A}}^{-1}\,\mathbf{G}_{\mathcal{C}}$ are derived.

Term M_{11}:

$$\begin{aligned} &\left(1+\frac{\epsilon^2}{2}\,\alpha^n\,(\omega_{\mathcal{A}}^0)^2\right)\left(1-\epsilon\,j\,\mathscr{C}_{|u|}-\frac{\mathscr{C}_{|u|}}{\mathscr{C}_{|u|}^{\text{crit}}}\frac{\epsilon^2}{2}\right)-\epsilon^2\,\mathscr{C}_{|u|}\frac{\rho^0\,(c_{\mathcal{C}}^0)^2}{|u^0|}\frac{\alpha^n}{a_{\mathcal{A}}^0}+O(\epsilon^3) \\ =&1-\epsilon\,j\,\mathscr{C}_{|u|}+\frac{\epsilon^2}{2}\left(\alpha^n\,(\omega_{\mathcal{A}}^0)^2-\frac{\mathscr{C}_{|u|}}{\mathscr{C}_{|u|}^{\text{crit}}}-2\,\mathscr{C}_{|u|}\frac{\rho^0\,(c_{\mathcal{C}}^0)^2}{|u^0|}\frac{\alpha^n}{a_{\mathcal{A}}^0}\right)+O(\epsilon^3). \end{aligned} \tag{70}$$

Term M_{22}:

$$\begin{aligned} &\left(1+\frac{\epsilon^2}{2}\,\alpha^n\right)\left(1-\epsilon\,j\,\mathscr{C}_{|u|}-\frac{\mathscr{C}_{|u|}}{\mathscr{C}_{|u|}^{\text{crit}}}\frac{\epsilon^2}{2}\right)-\epsilon^2\,\mathscr{C}_{|u|}\frac{(\mathscr{E}_0^n)^2}{\rho^0\;|u^0|}\alpha^n\,(\omega_{\mathcal{A}}^0)^2\,a_{\mathcal{A}}^0+O(\epsilon^3) \\ =&1-\epsilon\,j\,\mathscr{C}_{|u|}+\frac{\epsilon^2}{2}\left(\alpha^n-\frac{\mathscr{C}_{|u|}}{\mathscr{C}_{|u|}^{\text{crit}}}-2\,\mathscr{C}_{|u|}\frac{(\mathscr{E}_0^n)^2}{\rho^0\;|u^0|}\alpha^n\,(\omega_{\mathcal{A}}^0)^2\,a_{\mathcal{A}}^0\right)+O(\epsilon^3). \end{aligned} \tag{71}$$

It can be noticed that: $M_{22} = M_{11} + \epsilon^2\,\Delta M + O(\epsilon^3)$ with $\Delta M \in \mathbf{R}$ defined as:

$$\begin{aligned} \Delta M &= \left[\frac{\alpha^n\,(1-(\omega_{\mathcal{A}}^0)^2)}{2}-\Psi\right], \\ \Psi &= \frac{\alpha^n\,\mathscr{C}_{|u|}}{|u^0|}\left(\frac{(\mathscr{E}_0^n)^2\,(\omega_{\mathcal{A}}^0)^2\,a_{\mathcal{A}}^0}{\rho^0}-\frac{\rho^0\,(c_{\mathcal{C}}^0)^2}{a_{\mathcal{A}}^0}\right). \end{aligned} \tag{72}$$

Term M_{12}:

Directly:

$$-\epsilon\,j\,\left[\frac{(\mathscr{E}_0^n)^2\,\mathscr{C}_{|u|}}{\rho^0\;|u^0|}+\frac{\alpha^n}{a_{\mathcal{A}}^0}\right]-\epsilon^2\,\mathscr{C}_{|u|}\,\frac{\alpha^n}{a_{\mathcal{A}}^0}+O(\epsilon^3). \tag{73}$$

Term M_{21}:

Directly:

$$-\epsilon\, j\, \left[\frac{\rho^0\,(c_{\mathcal{C}}^0)^2\,\mathscr{C}_{|u|}}{|u^0|} + \alpha^n\,(\omega_{\mathcal{A}}^0)^2\,a_{\mathcal{A}}^0\right] - \epsilon^2\,\mathscr{C}_{|u|}\,\alpha^n\,(\omega_{\mathcal{A}}^0)^2\,a_{\mathcal{A}}^0 + O(\epsilon^3). \tag{74}$$

Derivation of the Eigenvalues

The eigenvalues of $\mathbf{G}_{\mathcal{A}}^{-1}\,\mathbf{G}_{\mathcal{C}}$ can be obtained by finding the roots of:

$$\begin{bmatrix} M_{11}-\lambda & M_{12} \\ M_{21} & M_{11}-\lambda+\epsilon^2\,\Delta M \end{bmatrix}. \tag{75}$$

One can notice that the order $O(\epsilon^2)$ in M_{12} and M_{21} will give a $O(\epsilon^3)$ contribution. Define $X = M_{11} - \lambda$. One has to solve:

$$\begin{aligned} &X^2 + \epsilon^2\,\Delta M\,X + \epsilon^2\,\left[(\mathscr{E}_0^n)^2\,\mathscr{C}_{|u|}^2\left(\frac{c_{\mathcal{C}}^0}{|u^0|}\right)^2 + (\alpha^n)^2\,(\omega_{\mathcal{A}}^0)^2 + \Phi\right] + O(\epsilon^3) = 0, \\ &\Phi = \frac{\alpha^n\,\mathscr{C}_{|u|}}{|u^0|}\left(\frac{(\mathscr{E}_0^n)^2\,(\omega_{\mathcal{A}}^0)^2\,a_{\mathcal{A}}^0}{\rho^0} + \frac{\rho^0\,(c_{\mathcal{C}}^0)^2}{a_{\mathcal{A}}^0}\right). \end{aligned} \tag{76}$$

If one neglects the order $O\left(\epsilon^3\right)$ terms in (76), the discriminant of the simplified polynomial function writes:

$$\begin{aligned} \Delta^d &= \epsilon^4\,(\Delta M)^2 - 4\,\epsilon^2\,\left[(\mathscr{E}_0^n)^2\,\mathscr{C}_{|u|}^2\left(\frac{c_{\mathcal{C}}^0}{|u^0|}\right)^2 + (\alpha^n)^2\,(\omega_{\mathcal{A}}^0)^2 + \Phi\right] \\ &= -4\,\epsilon^2\,\left[(\mathscr{E}_0^n)^2\,\mathscr{C}_{|u|}^2\left(\frac{c_{\mathcal{C}}^0}{|u^0|}\right)^2 + (\alpha^n)^2\,(\omega_{\mathcal{A}}^0)^2 + \Phi\right] + O(\epsilon^4). \end{aligned} \tag{77}$$

Thus Δ^d is negative for sufficiently small ϵ. One can approximate the roots as:

$$\begin{aligned} X^{\pm} &= -\epsilon^2\frac{\Delta M}{2} \pm |\epsilon|\; j\,X^0 + O(\epsilon^3), \\ X^0 &= \sqrt{(\mathscr{E}_0^n)^2\,\mathscr{C}_{|u|}^2\left(\frac{c_{\mathcal{C}}^0}{|u^0|}\right)^2 + (\alpha^n)^2\,(\omega_{\mathcal{A}}^0)^2 + \Phi}. \end{aligned} \tag{78}$$

It can be noticed that the order $O(|\epsilon|)$ contribution X^0 results from the product of the order $O(\epsilon)$ terms of M_{12} and M_{21}.

Finally, the roots of the von Neumann gain matrix are:

$$\begin{aligned}
\lambda^{\pm} &= \frac{1}{\Delta}\left(1+\frac{\epsilon^2}{2}(\Delta M+R) \mp |\epsilon|\; j\, X^0 - \epsilon\, j\, \mathscr{C}_{|u|} + O(\epsilon^3)\right),\\
R &= \left(\alpha^n\,(\omega_{\mathcal{A}}^0)^2 - \frac{\mathscr{C}_{|u|}}{\mathscr{C}_{|u|}^{\text{crit}}} - 2\,\mathscr{C}_{|u|}\frac{\rho^0\,(c_{\mathcal{C}}^0)^2}{|u^0|}\frac{\alpha^n}{a_{\mathcal{A}}^0}\right)
\end{aligned} \tag{79}$$

It can be noticed that the contribution of the determinant Δ only has an impact on the $O(\epsilon^2)$ terms, namely:

$$\begin{aligned}
\lambda^{\pm} &= 1+\frac{\epsilon^2}{2}(\Delta M+R-W) \mp |\epsilon|\; j\, X^0 - \epsilon\,\mathscr{C}_{|u|} + O(\epsilon^3),\\
R &= \left(\alpha^n\,(\omega_{\mathcal{A}}^0)^2 - \frac{\mathscr{C}_{|u|}}{\mathscr{C}_{|u|}^{\text{crit}}} - 2\,\mathscr{C}_{|u|}\frac{\rho^0\,(c_{\mathcal{C}}^0)^2}{|u^0|}\frac{\alpha^n}{a_{\mathcal{A}}^0}\right),\\
W &= \alpha^n\,\left(1+(\omega_{\mathcal{A}}^0)^2\,(1+2\,\alpha^n)\right).
\end{aligned} \tag{80}$$

A crucial point here is to note that the coefficient X^0 contains terms of order $O(1/M^0)$ since $(\omega_{\mathcal{A}}^0)^2$ is an order one term and α^n an order $O(1/M^0)$ term. Indeed after calculation, one can find a simpler expression for X^0:

$$\begin{aligned}
&X^0 = \frac{\mathscr{C}_{|u|}}{|u^0|}\sqrt{(c_{\mathcal{C}}^0)^2+(1-(\mathscr{E}_0^n)^2)\left(\frac{a_{\mathcal{A}}^0}{\rho^0}\right)^2(\omega_{\mathcal{A}}^0)^2} = \frac{\mathscr{C}_{|u|}}{|u^0|}\sqrt{(c_{\mathcal{C}}^0)^2+(1-(\mathscr{E}_0^n)^2)\,(c_{\mathcal{A}}^0)^2} = \frac{\mathscr{C}_{|u|}}{M^0},\\
&\text{since: } (c_{\mathcal{C}}^0)^2+\left(1-(\mathscr{E}_0^n)^2\right)(c_{\mathcal{A}}^0)^2 = (c^0)^2.
\end{aligned} \tag{81}$$

We think that the $|\epsilon|\; X^0$ contribution in the imaginary part of the gain matrix eigenvalues is responsible for the decay of the upper bound of the stable convective Courant number $\mathscr{C}_{|u|}$.

References

[1] L. Allievi. Teoria generale del moto perturbato dell'acqua nei tubi in pressione (coplo d'ariete). *Tip. del Genio civile*, 1902.

[2] W. F. Ballhaus and P. M. Goorjian. Implicit finite-difference computations of unsteady transonic flows about airfoils. *AIAA Journal*, 15:1728–1735, 1977.

[3] W. F. Ballhaus and P. M. Goorjian. Implicit methods of second-order accuracy for the Euler equations. *AIAA Journal*, 23:33–40, 1985.

[4] R. Baraille, G. Bourdin, F. Dubois, and A. Y. Le Roux. Une version à pas fractionnaires du schéma de Godunov pour l'hydrodynamique. *Compte Rendu de l'Académie des Sciences*, 314:147–152, 1992.

[5] F. Bouchut. Entropy satisfying flux vector splittings and kinetic BGK models. *Numerische Mathematik*, 94:623–672, 2003.

[6] F. Bouchut. *Nonlinear Stability of Finite Volume Methods for Hyperbolic Conservation Laws*. Birkäser, 2004.

[7] C. Chalons, M. Girardin, and S. Kokh. An all-regime Lagrange-Projection like scheme for 2D homogeneous models for two-phase flows on unstructured meshes. *Journal of Computational Physics*, 335:885–904, 2016.

[8] C. Chalons, M. Girardin, and S. Kokh. An all-regime Lagrange-Projection like scheme for the gas dynamics equations on unstructured meshes. *Communications in Computational Physics*, 20:188–233, 2016.

[9] S. Clerc. Numerical simulation of the homogeneous equilibrium model for two-phase flows. *Journal of Computational Physics*, 161:354–375, 1999.

[10] F. Coquel, E. Godlewski, and N. Seguin. Relaxation of fluid systems. *Mathematical Models and Methods in Applied Science*, 22:43–95, 2012.

[11] F. Coquel, Q. L. Nguyen, M. Postel, and Q. H. Tran. Entropy-satisfying relaxation method with large time-steps for Euler IBVPS. *Mathematics of Computation*, 79:1493–1533, 2010.

[12] F. Daude, I. Mary, and P. Comte. Self-adaptative Newton-based iteration strategy for the LES of turbulent multi-scale flows. *Computers and Fluids*, 100:278–290, 2014.

[13] P. Degond and M. Tang. All speed scheme for the low Mach number limit of the isentropic Euler equation. *Communications in Computational Physics*, 10:1–31, 2011.

[14] S. Dellacherie, P. Omnes, J. Jung, and P.A. Raviart. Construction of modified Godunov type schemes accurate at any Mach number for the compressible Euler system. *Mathematical Models and Methods in Applied Science*, 26:2525–2615, 2016.

[15] G. Dimarco, R. Loubère, and M-H. Vignal. Study of a new asymptotic preserving scheme for the Euler system in the low Mach number limit. *Preprint*, https://hal.archives-ouvertes.fr/hal-01297238, 2016.

[16] T. Gallouët, J-M Hérard, and N. Seguin. A hybrid scheme to compute contact discontinuities in one-dimensional Euler systems. *ESAIM: Mathematical Modelling and Numerical Analysis*, 36:1133–1159, 2002.

[17] M. S. Ghidaoui, M. Zhao, D. A. McInnis, and D. H. Axworthy. A review of water hammer theory and practice. *Applied Mechanics Reviews*, 58:49, 2005.

[18] M. Girardin. *Asymptotic preserving and all-regime Lagrange-Projection like numerical schemes: application to two-phase flows in low Mach regime*. PhD thesis, Université Pierre et Marie Curie, https://tel.archives-ouvertes.fr/tel-01127428, 2015.

[19] H. Guillard and A. Murrone. On the behavior of upwind schemes in the low Mach number limit: II Godunov type schemes. *Computers and Fluids*, 33:655–675, 2004.

[20] H. Guillard and C. Viozat. On the behavior of upwind schemes in the low Mach number limit. *Computers and Fluids*, 28:63–86, 1999.

[21] J. Haack, S. Jin, and J. G. Liu. An all-speed asymptotic-preserving method for the isentropic Euler and Navier-Stokes equations. *Communications in Computational Physics*, 12:955–980, 2012.

[22] T. Y. Hou and P. G. Le Floch. Why nonconservative schemes converge to wrong solutions: error analysis. *Mathematics of computation*, 62:497–530, 1994.

[23] D. Iampietro, F. Daude, P. Galon, and J. M. Hérard. A Mach-sensitive splitting approach for Euler-like systems. https://hal.archives-ouvertes.fr/hal-01466827, 2017.

[24] S. Jin. Efficient asymptotic-preserving (AP) schemes for some multiscale kinetic equations. *SIAM Journal on Scientific Computing*, 21:441–454, 1999.

[25] N. E. Joukowski. Memoirs of the Imperial Academy Society of St. Petersburg. *Proceedings of the American Water Works Association*, 24:341–424, 1898.

[26] M. P. Martín and G. V. Candler. A parallel implicit method for the direct numerical simulation of wall-bounded compressible turbulence. *Journal of Computational Physics*, 215:153–171, 2006.

[27] G. R. McGuire and J. L. Morris. A class of implicit, second-order accurate, dissipative schemes for solving systems of conservation laws. *Journal of Computational Physics*, 14:126–147, 1974.

[28] G. R. McGuire and J. L. Morris. Explicit-implicit schemes for the numerical solution of nonlinear hyperbolic systems. *Mathematics of Computation*, 29:407–424, 1975.

[29] A. Murrone and H. Guillard. Behavior of upwind scheme in the low Mach number limit: III. Preconditioned dissipation for a five equation two phase model. *Computers and Fluids*, 37(10):1209–1224, 2008.

[30] S. Noelle, G. Bispen, K. R. Arun, M. Lukáčová-medviďová, and C. D. Munz. A weakly asymptotic preserving low Mach number scheme for the Euler equations of gas dynamics. *SIAM Journal on Scientific Computing*, 36:B989–B1024, 2014.

[31] J. Schütz and S. Noelle. Flux splitting for stiff equations: a notion on stability. *Journal of Scientific Computing*, 64:522–540, 2015.

[32] A. R. Simpson and E. B. Wylie. Large water-hammer pressures for column separation in pipelines. *Journal of Hydraulic Engineering*, 117:1310–1316, 1991.

[33] I. Suliciu. On the thermodynamics of fluids with relaxation and phase transitions. *International Journal of Engineering Science*, 36:921–947, 1998.

[34] E. Turkel. Preconditioned methods for solving the incompressible and low speed compressible equations. *Journal of Computational Physics*, 72:277–298, 1987.

[35] J. B. Whitham. *Linear and Non Linear Waves*. John Wiley & Sons Inc, 1974.

[36] H. Zakerzadeh. On the Mach-uniformity of the Lagrange–projection scheme. *ESAIM: Mathematical Modelling and Numerical Analysis*, 2016.

[37] H. Zakerzadeh and S. Noelle. A note on the stability of implicit-explicit flux splittings for stiff hyperbolic systems. *Preprint IGPM*, 2016.